International Journal of Rotating Machinery
1995, Vol. 1, No. 2, pp. 83–116
Reprints available directly from the publisher
Photocopying permitted by license only

Modal Testing of Rotors with Fluid Interaction

AGNES MUSZYNSKA
Bently Rotor Dynamics Research Corporation, Minden, NV 89423

Modal testing of rotating structures has specific aspects, and it requires a specialized approach. Classical modal testing when applied to active (rotating) structures does not provide complete results. These aspects, and specific application of sweep frequency circular input force perturbation testing of rotors rotating in fluid environment, are discussed in this paper.

Emphasis is placed on nonsynchronous perturbation of shafts rotating at a constant rotative speed. The results are presented in the direct and quadrature dynamic stiffness versus perturbation frequency formats, which permits the separation of components for easy evaluation. This perturbation technique provided new results: 1) identification of solid/fluid interaction modes; 2) identification of fluid dynamic forces in lightly loaded bearings and seals; and 3) multimode identification of rotor systems. Results of several laboratory rig experiments, the identification algorithm, and data processing techniques are discussed. A comparison with other testing methods is given.

Key Words: *Modal testing; rotor/bearing/seal systems; dynamic stiffness, parameter identification; fluid/solid interaction modes*

EXPERIMENTAL modal analysis has become a popular method for studying practical vibration problems of mechanical structures. Application of modal testing for parameter identification of rotating machines, which represent an important class of mechanical structures, has several specific aspects and requires a specialized approach. The results and predictions obtained by applying the classical "passive structure" modal testing to a rotating machine are usually incomplete, and not sufficiently accurate for the most important lateral modes, while providing information not significant for the rotating machine operating performance.

SPECIFIC ASPECTS OF MODAL TESTING OF ROTATING MACHINES

Most of the modal identification methods and conventional procedures of modal analysis deal with structures with assumed linear behavior. The structures are modeled by self-adjoint differential operators, and discretized by symmetric matrices. Rotating machines have an inherent nonsymmetric nature, due to rotation-related factors, such as gyroscopic effects, and fluid dynamic forces in bearings and seals, which provide feedback-like effects. The dynamic behavior of rotating machines can adequately be represented only by the *nonself-adjoint* differential operators. The discretization yields nonsymmetric matrices. The modal analysis must not only determine all classical modal parameters (for example, eigenvalues, eigenfunctions constituting the right eigenvectors and form of eigenfunctions yielding generalized/modal masses associated with each eigenmode), but also the parameters provided by the *left eigenfunctions.* Decoupling of rotor precessional mode components requires the utilization of additional relations (such as biorthogonality) between left and right eigenvectors (Childs [1976], Glasgow *et al.* [1980], Bigret [1984], Andrews [1985], Zhang *et al.* [1985]).

Rotating machines can be modeled by linear equations in very limited ranges of deflections and velocities. The classical modal analysis, based on the assumption of linearity, has to be completed by taking *nonlinearities* into consideration. Significant nonlinear effects of geometric and physical origin in rotating machines can introduce large errors on the classical modal tests (Black *et al.* [1980], Fillod *et al.* [1985], Sullivan [1985]).

All dynamic phenomena occurring during the performance of a rotating machine are closely related to the rotative motion of the rotor (Fig. 1). The continuous supply

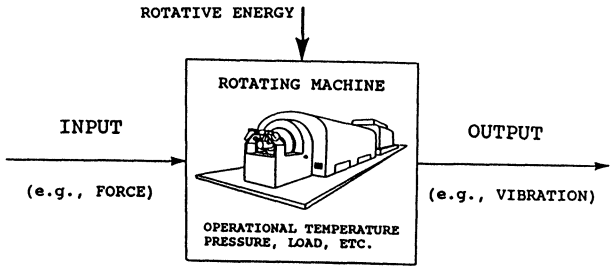

FIGURE 1 Perturbation technique for modal testing of rotating machines at their operational conditions.

of rotative energy makes the system "active," containing a feedback loop. Numerous vibrational phenomena in rotating machines occur due to the transfer of energy from *rotation* (main performance) to vibration (undesirable side effects). Rotation of the shaft with all mechanical parts attached to it, as well as involvement in rotation of the working fluid (in fluid-flow machines, in seals, and in bearings), causes important modifications in modes and natural frequencies. In large turbomachines, additional changes can be generated by thermal effects, foundation deformations, and misalignment. All these factors cause the results of modal testing of rotating machines "at rest" ("passive structure" approach) to differ significantly from the results of testing during machine operational conditions ("active structure" approach).

Rotors, which represent the main parts of rotating machines, are similarly constrained in two lateral directions; therefore, they exhibit vibrational motion which always has two inseparably coupled, two-orthogonal lateral components (conventionally called "vertical" and "horizontal"). The lateral vibrations result in *two-dimensional* precessional motion of the rotor. Widely used unidirectional impulse testing, when applied to a rotating shaft, results in a response containing vertical and horizontal components, and an undetermined tangential input force components.

In practical performances of rotors, the precessional motion can contain multi-frequency, two-dimensional components, with definite relations to the direction of rotation. In the most general case, each individual component can be either *forward* (direction of precession the same as direction of rotation) or *backward* (direction of precession opposite to rotation). The direction of precessional motion is vital to the rotor integrity, as it determines the rotor stress/deformation pattern. The net deformation frequency of the rotor is equal to the difference between rotative and precessional frequencies, with their signs taken into account. During backward precession the shaft is therefore subject to high frequency deformation (sum of both frequencies). When measuring rotating machine vibrations, it is important to identify each vibrational frequency component, whether it is forward or backward. Narrow band filtering, and time base/orbit analysis, are extremely helpful for this purpose. In classical modal testing, "negative" frequencies have no meaning. Applied to rotating machines, the "negative" frequency has a direct, and very significant physical interpretation related to rotor backward precession.

Most important vibrational phenomena of rotating machines are associated with rotor lateral vibrations. Each mode of rotor lateral vibration contains two components (vertical and horizontal), the characteristics of which are, usually, slightly different as a result of elasticity/mass nonsymmetry of the rotor, and supporting structure, in two orthogonal lateral directions. Modal testing of structures with *closely spaced* modes presents numerous difficulties. Rotating machines belong to this category. An alleviation of the problem is offered by consideration of "pair modes" in rotating machines (for example, "first mode vertical" and "first mode horizontal").

Classical modal testing usually, though not always, deals with a large number of modes of a structure over a broad frequency range. In the performance of rotating machines, the most important are the *lowest modes,* and low-frequency precessional phenomena. This is because: first, the stiffness/mass characteristics of a rotor are always located in a lower range of frequencies than those of the supporting structure. The lowest modes of the rotating machine correspond, therefore, to the modes of the rotor itself. Second, the rotating machine has its own continuously active forcing function—the unbalance, which is an inseparable feature of the rotating system. The frequency of this force is equal to the rotor's actual rotative speed. The resulting motion is referred to as a "synchronous" precession. The operating speed of a single-span machine train, even if it represents dozens of thousands of rpm, seldom exceeds the third balance resonance frequency (third lateral natural frequency); therefore, main interest should be concentrated on investigating the rotor's first two or three lateral/bending modes, because the rotating machine has to survive resonant conditions of the lowest modes during each start-up and shutdown. The amplitudes of rotor deformations at low modes are the highest, and the low modes are usually poorly damped; therefore, they are of the greatest concern.

There is one more aspect of importance, focused on the rotor lowest modes. Almost all self-excited vibrational/precessional phenomena occurring during the performance of a rotating machine are characterized by low frequencies that are always located in the *subsynchronous* region (frequencies lower than the synchronous frequency). The self-excited vibrations usually occur

when rotative speed is sufficiently high, and when there exists a mechanism that transfers rotative energy into self-excited vibrations. The latter are often referred to as "rotor instabilities" (instability of the pure rotative motion after an onset of instability, with an immediately following, limit cycle of self-excited vibrations). The frequency of self-excited vibrations is either equal to a fraction of the actual rotative speed, with the same ratio to rotative speed maintained if the rotative speed varies (for example, oil whirl, partial rub), or it is rotative speed independent, and close to any rotor bending mode natural frequency (for example, oil whip, full annular rub). Most often, due to a specific role of rotor internal/structural friction, the subsynchronous vibrations of rotating machines are characterized by much higher amplitudes than supersynchronous vibrations.

When dealing with a high number of modes during classical modal testing, the accuracy of the phase angle readings is usually low. In rotating machines the *phase angle* represents an extremely important parameter. It not only gives information on the force/response relationship, but also relates the shaft lateral vibration to its rotative motion. It also yields significant information in modal parameter identification procedures. By limiting modal testing to the lowest modes, it is possible to increase the accuracy of phase angle measurements.

Finally, the most important aspect: the results of the modal testing of rotors at their operational conditions reveal the existence of *specific modes,* unknown in "passive" structures. These modes are generated by solid/fluid interaction, activated by the shaft rotation, such as in fluid-lubricated bearings and seals. During the rotating machine performance, these modes exhibit their activity through rotor self-excited vibrations (for example, "oil whirl" is the rotor/bearing system self-excited vibration; "oil whirl resonance," "oil whirl natural frequency," and "oil whirl mode" are modal parameters of the rotor/bearing system revealed by perturbation testing, as discussed by Bently *et al.* [1982b, 1985c], and Muszynska [1986].

In summary, modal analysis of rotating machines provides a significant computational complexity due to the nonsymmetric nature of rotating structure dynamic behavior. Modal testing of rotating machines should be focused on the rotor lowest bending modes, and applied to the rotor during normal operational conditions of the rotating machine.

The classical modal testing, as used in case of "passive" structures, is not the most efficient for this purpose. Better results can be obtained by applying limited frequency sweep, circular-force, *perturbation testing,* which will be discussed in the next section.

INPUT FUNCTIONS USED IN MODAL TESTING OF ROTATING MACHINES

Classical modal testing uses unilateral exciting forces, such as provided by hammer impacting or shaker sinusoidal excitation. Static structures exhibit symmetry (in terms of the mathematical model, all matrices are symmetric), which results in reciprocity of the cross-data: accelerance at point "p" when force is applied at point "r" is equal to the accelerance at point "r" when force is applied at point "p".

Rotors are not symmetric. Nonsymmetry in the system matrices results from rotation-generated tangential forces. The natural frequencies and lateral modes are different for each direction of rotation. They are referred to as "forward" and "backward" modes. Their corresponding natural frequencies differ in values, and these differences are functions of rotative speed. Some other operational factors may also contribute to the differences.

When the classical unilateral excitation is applied to a rotating shaft, the forced response consists of both forward and backward modes, which are difficult to separate. The best excitation for rotating shaft modal testing during machine operational conditions is a *rotating* circular force with distinct direction: forward (same as rotation) or backward (opposite to rotation). This type of nonsynchronous excitation allows for the easy separation of the forward and backward lateral modes, and the identification of rotation-generated terms (Stone *et al.* [1947]; Hull [1955]; Bently *et al.* [1979, 1982a,b, 1983, 1984, 1985a,b,c, 1986]). Muszynska [1986]). The term "nonsynchronous" refers to the perturbation frequency which is different from the rotative speed.

The use of a circular rotating input force perturbation system has further advantages, namely, and ease of controlling the frequency, force magnitude, and phase, by using, for instance, a controlled unbalance.

Various types of perturbation systems generating rotating forces can be applied, such as: A) an unbalanced rotating free spinner mounted on the shaft and driven by a compressed air jet flow; B) an unbalanced auxiliary shaft attached to the end of the rotating machine rotor through a pivoting bearing, and driven by a separate motor; both A) and B) allow for shaft "nonsynchronous" perturbation (Fig. 2). Two electromagnetic actuators in XY configuration generating sinusoidal forces with 90-degree phase shift can also be applied as input circular force perturbators. Another device which provides a perturbation frequency-independent input force amplitude consists of radial spring-like elastic elements attached from one end to the rolling element bearing mounted on the rotor.

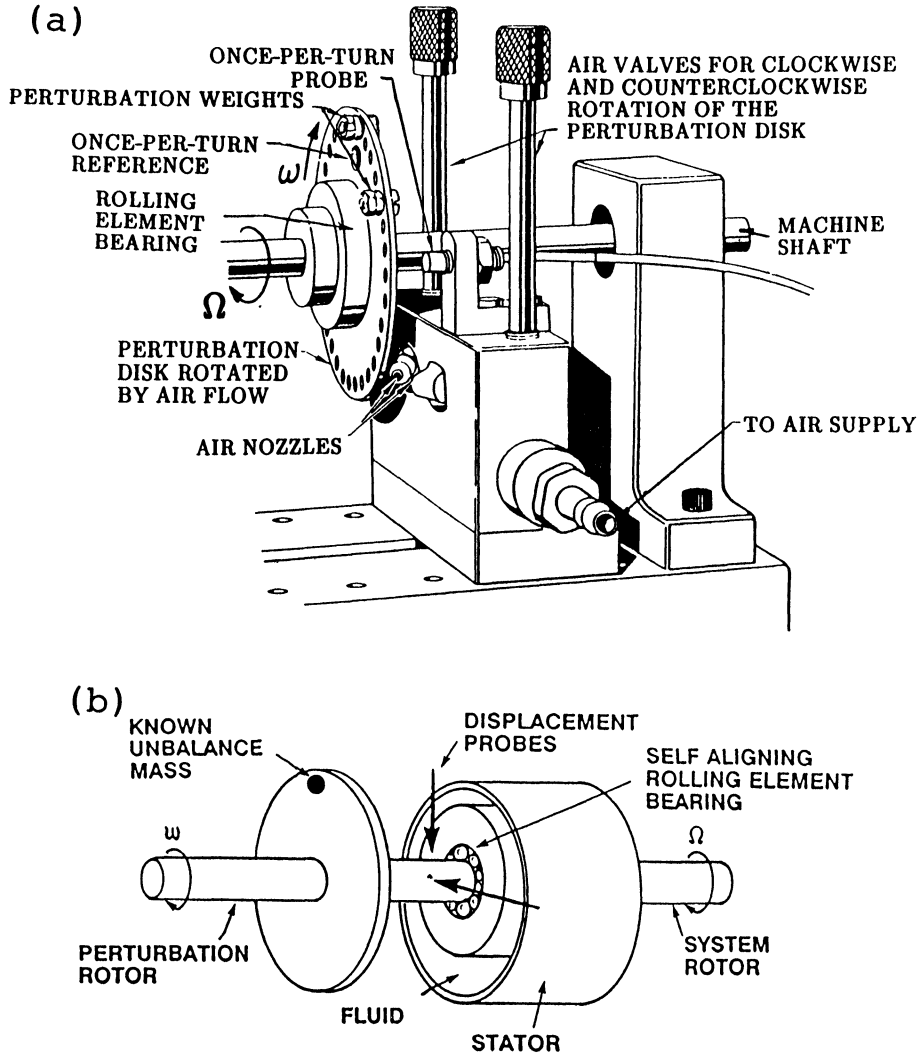

FIGURE 2 Perturbation testing of rotating machines using sweep frequency circular forces generated by rotating unbalance at (a) free spinner; or (b) rigid auxiliary rotor. Rotative speed of the main shaft (Ω) maintained constant.

On the other ends the springs are mounted in a nonsynchronously rotating and (due to its eccentricity) oscillating ring (Fig. 3). This device provides a good resolution in low frequency range testing.

In all these systems, the frequency (angular speed) of the perturbing force is entirely independent from the rotative speed of the main shaft: the latter rotates at a chosen constant speed, while the perturbator provides the input rotating force with sweep frequency. The shaft can be perturbed either in a forward or a reverse direction. These perturbation systems also yield very good results in "passive".

In all above-mentioned methods, as well as other popular modal testing routines (such as impulse testing), the input into the system is a force; the output is a measured response in terms of mechanical displacement, velocity, or acceleration. There exists a method applied in rotating systems with fluid interactions, in which a displacement is used as an input, and the force is measured at the output (Iwatsubo *et al.* [1980, 1988], Ohashi *et al.* [1984, 1988], Jery *et al.* [1984], Adkins *et al.* ([986], Childs *et al.* [1986, 1988], Kanki *et al.* [1986], Adams *et al.* [1988], Brennen *et al.* [1988]). The forced circular displacement in an orbital form is generated by a cam mechanism on the shaft rotating in a fluid environment. The output fluid dynamic force is calculated from the pressure transducer or load cell readings (Fig. 4). This method provides nonsynchronous perturbation; it is used for identification of fluid dynamic forces in seals and fluid-handling machines. A comparison of results yielded by this method, and the input force/output displacement method is given

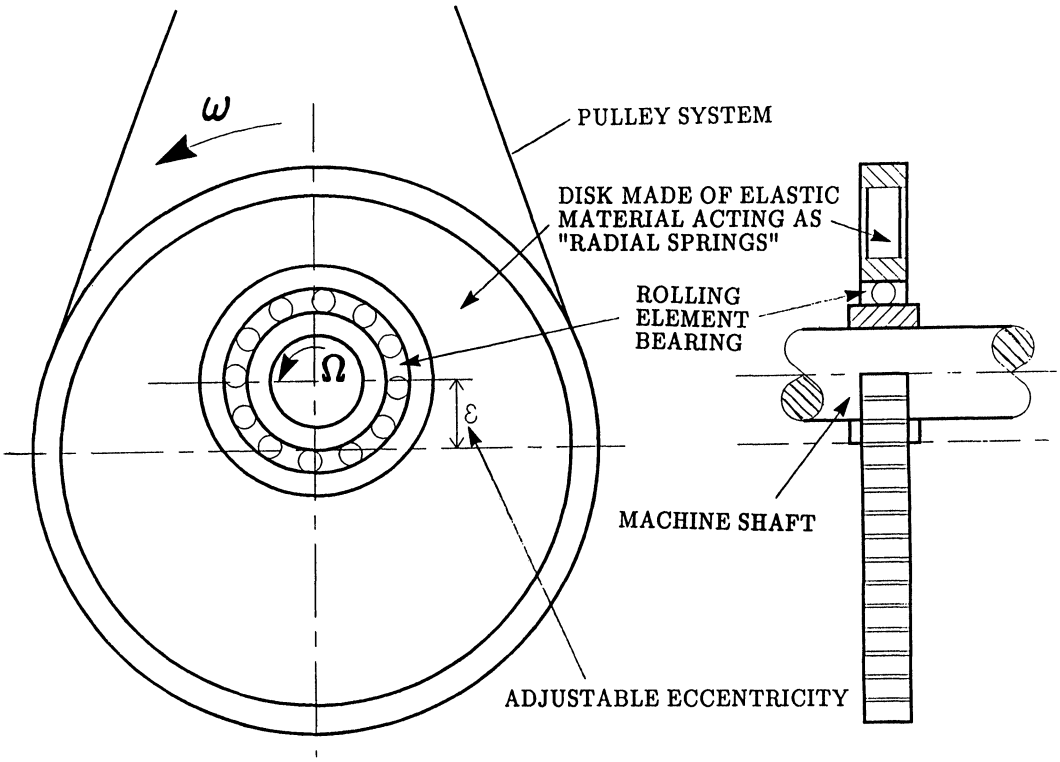

FIGURE 3 Constant force amplitude perturbation device (eccentricity exaggerated).

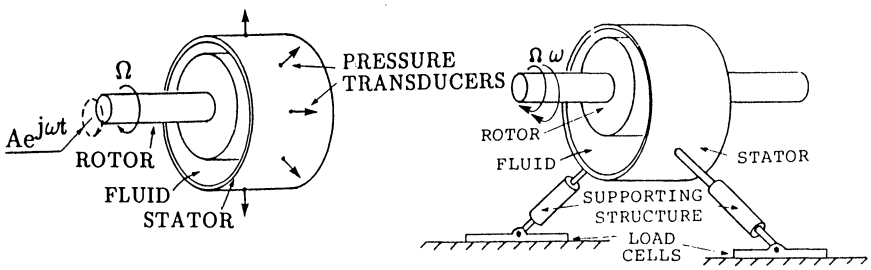

FIGURE 4 Rotating displacement input and fluid pressure (a) or load cell; (b) output perturbation method.

in the section where perturbation results are compared (see p. xxx).

RESPONSE MEASUREMENTS

Accelerometers are the most popular transducers used in classical modal testing. The testing results are presented in terms of accelerances (or "inertances") which are the ratios of response acceleration vectors to input force vectors ("vector" means amplitude and phase of a harmonic variable). Accelerometers are the most appropriate instruments for modal testing of passive structures, which deals usually with high number of modes, with natural frequencies located in a relatively broad frequency range.

In a rotating machine the modes of highest interest are those of the rotor itself. Most often the rotor modes correspond to the *lowest* modes of the entire machine structure. The first natural frequency may occur in the range of 5 to 15 Hz. In this range of frequencies accelerometers perform very poorly. The best transducer in the low frequency range is the displacement proximity probe. When mounted in casings or bearings, the proximity probe provides relative measurements (shaft motion *relative* to support motion). For machines with very soft supports the proximity probe can be complemented by a seismic probe providing casing *absolute* measurements (for instance, a dual transducer).

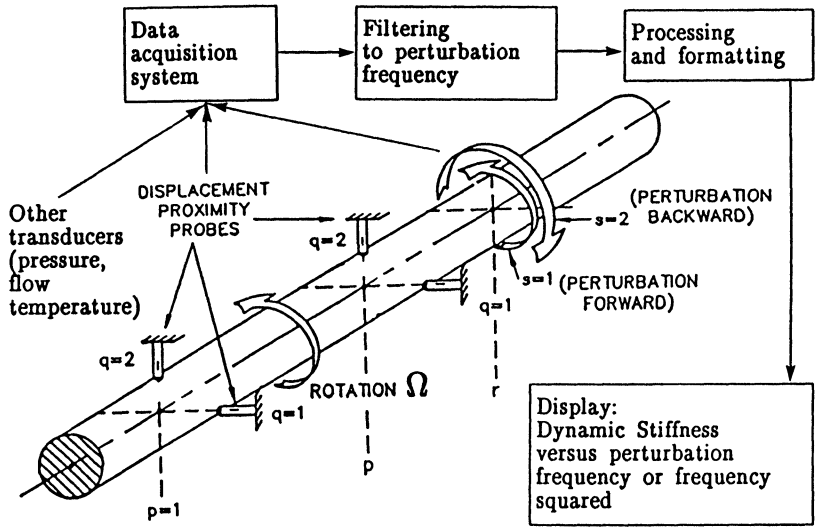

FIGURE 5 Modal testing of a rotating shaft using circular forward and backward perturbation forces and displacement noncontacting proximity transducers for vibration response measurements.

Results of modal testing using displacement transducers are usually presented in terms of receptances (there exists in the literature equally used names, such as "admittances," "compliances," "dynamic flexibilities"). The receptances are the ratios of the displacement response vectors to input force vectors. Receptance vectors are widely used, for instance, in rotor balancing. (They are often called "influence coefficients," but the more proper name should be *"influence vectors."*)

The use of accelerometers, velocity pickups, or proximity transducers in measurements of mechanical structure vibrations is not only a matter of rational choice, corresponding by matching the best to the type of encountered conditions, it is also a matter of philosophical usage—although popular in modal analysis applications, accelerometers are not widely used in on-line monitoring and diagnostics of rotating machinery malfunctions. Rotor displacements, not accelerations, are the most meaningful signals for the operating personnel.

Specific changes in rotor displacements (vibration amplitudes, as well as static positions) relative to machine casing directly indicate what type of malfunctions the machine develops. Changes in the static positions indicate changes in the alignment state. These data assist in prediction of fluid whirl/whip self-excited vibrations, as well as shaft crack prevention. A specific content of vibration signals indicates presence of unbalance, misalignment, rotor-to-stator rubs, loose parts, shaft crack propagation, and other malfunctions of the rotating machine.

The most harmful vibrations for the integrity of the rotating machine are *low* frequency, subsynchronous vibrations, resulting usually from an instability action transferring rotational energy into vibrations. Acceleration amplitudes are proportional to the square of vibration frequency. This means that when measuring rotor vibration by using accelerometers, the higher frequency components become dominant, indicating high amplitudes. The low frequency components look insignificantly small, even though they might have very high amplitudes in terms of rotor displacements. In addition, accelerometers are most often installed outside the rotor casing; thus they measure vibrations of the outside structure, not the vibrations of the rotor, which is the main source of vibration. During transmission from the source through the structure, vibration becomes attenuated, the degree of attenuation depending on the structure transmissibility.

In summary, in the rotating machine perturbation testing, the most useful instruments to measure rotor responses are displacement transducers mounted in *XY* configuration (Fig. 5), with a Keyphasor® once-per-turn marker for phase reference.

NONSYNCHRONOUS SWEEP FREQUENCY PERTURBATION TESTING AND DYNAMIC STIFFNESS IDENTIFICATION ALGORITHM

In the classical modal testing, identification of the structure modal parameters is usually based on curve fitting of results presented in the form of receptances (Ewins, [1984], Fig. 6). Much better identification results are

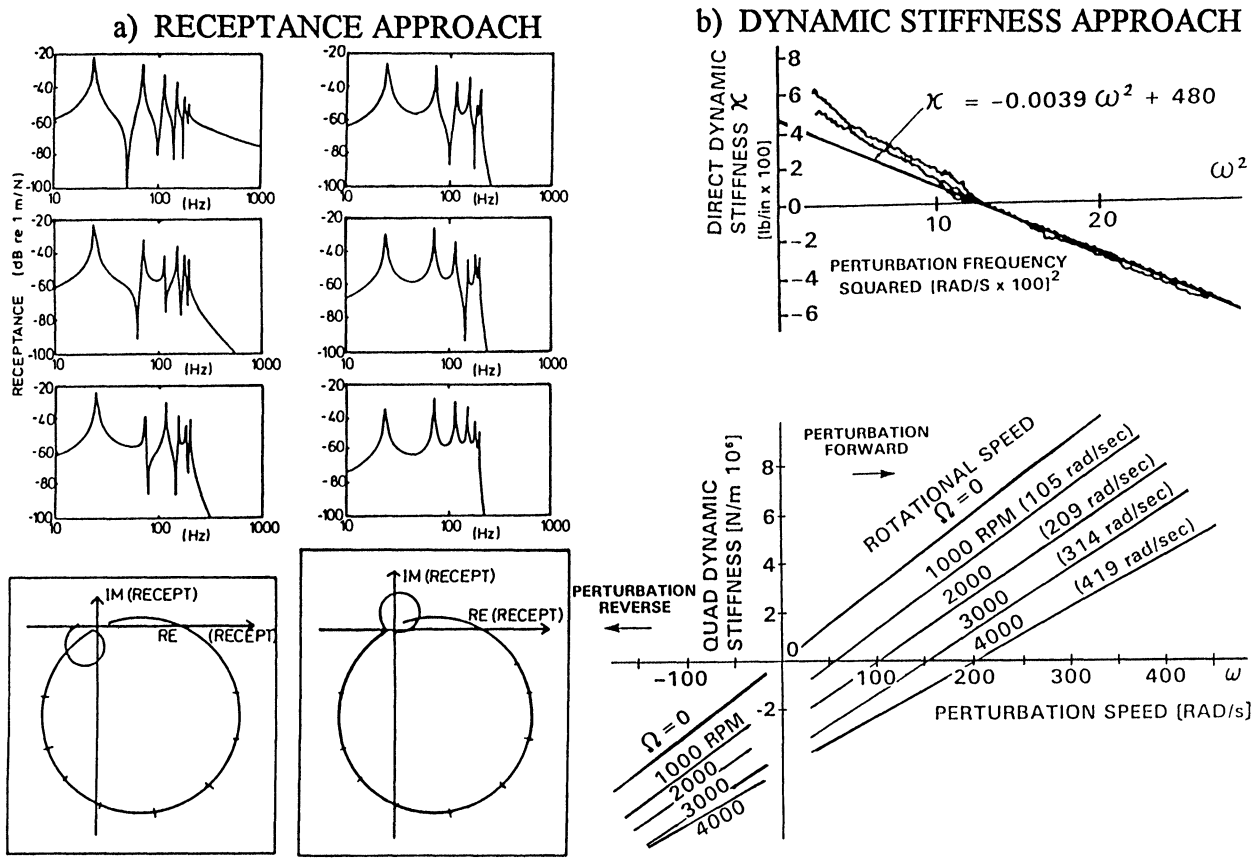

FIGURE 6 Identification of modal parameters: (a) curve fitting of receptances (Ewins [1984]); (b) straight-line fitting of dynamic stiffness results (Muszynska [1986]).

obtained, however, when a Dynamic Stiffness approach is applied. Straight lines of dynamic stiffness components are definitely the best to fit. A dynamic stiffness algorithm for identification of modal parameters of a rotating machine rotor using nonsynchronous sweep frequency perturbation testing is outlined below.

Rotor responses to rotating force excitation bring meaningful data for identification of the system parameters. The identification procedure involves matrix inversion, thus a computer is necessary for experimental data acquisition and processing.

Consider a modal of a nonsymmetric (laterally anisotropic), anisotropically supported, flexible $2n$ degree of freedom ($2n$ lateral mode) rotor rotating at a constant speed Ω (Fig. 5):

$$\begin{bmatrix}[M_1][M_{12}]\\ [M_{21}][M_2]\end{bmatrix}[\ddot{Z}] + \begin{bmatrix}[D_1][D_{12}]\\ [D_{21}][D_2]\end{bmatrix}[\dot{Z}] + \begin{bmatrix}[K_1][K_{12}]\\ [K_{21}][K_2]\end{bmatrix}[Z] = [F] \qquad \bullet = d/dt \quad (1)$$

where $Z = \text{col}[x_1, \ldots, x_p, \ldots, x_n, y_1, \ldots, y_p, \ldots, y_n]$ represents rotor deflections at its $p = 1, \ldots, n$ axial locations in two orthogonal directions x and y. The system parameters are represented by the matrices:

$$[M_q], [M_{q,3-q}], [D_q], [D_{q,3-q}], [K_q], [K_{q,3-q}], \quad q = 1, 2,$$

which are inertia, damping, and stiffness matrices correspondingly. The matrices $[D_{q,3-q}]$ contain "cross" damping terms, matrices $[K_{q,3-q}]$ contain elements of the "cross" stiffness type. Both these matrices usually depend on the rotative speed Ω. The vector $[F]$ contains controlled perturbation (excitation) forces. For identification of the system parameters, a controlled rotating perturbation force is applied consecutively at "r" ($r = 1, \ldots, n$) axial locations of the rotor in either forward ($s = 1$) or backward ($s = 2$) direction. The "n" pairs of displacement transducers in an XY configuration are mounted at "p" ($p = 1, \ldots, n$) axial locations of the rotor (Fig. 5). When the force is applied at the rth location, the excitation

vector used in nonsynchronous perturbation is, therefore,

$$[F] = \text{col}[0, \ldots, 0, F_{sr}\cos(\omega t + \delta_{sr}), 0, \ldots, 0, (-1)^{s+1} \times F_{sr}\sin(\omega t + \delta_{sr}), 0, \ldots, 0], s = 1, 2 \quad (2)$$

where ω is perturbation frequency, F_{sr} and δ_{sr} are the perturbation force amplitude and phase, respectively. Note that the perturbation frequency ω is entirely independent from the rotative speed Ω.

The rotor forced response to exciting force (2) based on model (1) is as follows:

$$[Z] = \text{col}[A_{1s1r}\cos(\omega t + \alpha_{1s1r}), \ldots, A_{1snr}\cos(\omega t + \alpha_{1snr}), A_{2s1r}\sin(\omega t + \alpha_{2s1r}), \ldots, A_{2snr}\sin(\omega t + \alpha_{2snr})] \quad (3)$$

where A_{qspr}, α_{qspr} are amplitudes and phases of the responses, narrow-band filtered to the perturbation frequency. All phases are measured from the same once-per-rotation marker. By substituting (3) into Eqs. (1), eliminating time-related functions, and using Euler's complex number transformations, the algebraic set of $2n$ equations is obtained:

$$[\kappa]\begin{bmatrix}[A_{1spr}e^{j\alpha_{1spr}}]\\ [A_{2spr}e^{j\alpha_{2spr}}]\end{bmatrix} = F_{sr}e^{j\delta_{sr}}\{\text{col}[0, \ldots, 0, 1, 0, \ldots, 0, (-1)^{s+1}, 0, \ldots, 0]\} \quad (4)$$

where $j = \sqrt{-1}$ and

$$[\kappa] = \begin{bmatrix}[K_1]+j\omega[D_1]-\omega^2[M_1] & -j([K_{12}]+j\omega[D_{12}]-\omega^2[M_{12}])\\ j([K_{21}]+j\omega[D_{21}]-\omega^2[M_{21}]) & [K_2]+j\omega[D_2]-\omega^2[M_2]\end{bmatrix}$$

is the system complex dynamic stiffness matrix. The nonzero components at the right side of Eq. (4) are at the rth and $(n + r)$th rows.

For the sequence of n experiments, in which the force is applied consecutively at $r = 1, 2, \ldots, n$ locations, first in forward ($s = 1$) then in backward ($s = 2$) directions, the set of $2n$ equations is obtained:

$$[\kappa]\begin{bmatrix}[A_{11}] & [A_{12}]\\ [A_{21}] & [A_{22}]\end{bmatrix} = \begin{bmatrix}[F_1] & [F_2]\\ [F_1] & [-F_2]\end{bmatrix} \quad (5)$$

where

$$[A_{qs}] = \begin{bmatrix}\bar{A}_{qs11} & \cdots & \bar{A}_{qs1n}\\ \vdots & & \vdots\\ \bar{A}_{qsn1} & \cdots & \bar{A}_{qsnn}\end{bmatrix} \equiv [A_{qspr}e^{j\alpha_{qspr}}], \quad (6)$$

$$F_s = \text{diag}[F_{s1}e^{j\delta_{s1}}, \ldots, F_{sn}e^{j\delta_{sn}}], \quad q, s = 1, 2$$

In Eq. (6) $\bar{A}_{qspr} \equiv A_{qspr}e^{j\alpha_{qspr}}$, $q, s = 1, 2$, $p, r = 1, \ldots, n$ represent response vectors (in complex number sense), components of the response nonsingular matrix. Note that the number of tests ($2n$) must correspond to the number of identified modes, thus certain knowledge on the system behavior is required ahead of time, to avoid singularity of the matrix $[A_{qs}]$. Equation (5) yields the main equation for identification of the system parameters:

$$[\kappa] = \begin{bmatrix}[F_1] & [F_2]\\ [F_1] & [-F_2]\end{bmatrix}\begin{bmatrix}[A_{11}] & [A_{12}]\\ [A_{21}] & [A_{22}]\end{bmatrix}^{-1} \quad (7)$$

The identification procedure is reduced to the following expressions, representing the rotor dynamic stiffness components:

$$[K_q] - \omega^2[M_q] = -\text{Re}\{[(-1)^q[F_2] + [H_1]][H_2]\};$$
$$\omega[D_q] = -\text{Im}\{[(-1)^q[F_2] + H_1]][H_2]\}; \quad (8)$$
$$\omega[D_{3-q,q}] = \text{Re}\{[(-1)^q[F_2] - [H_1]][H_2]\};$$
$$[K_{3-q,q}] - \omega^2[M_{3-q,q}] = \text{Im}\{[(-1)^q[F_2] - [H_1]][H_2]\}; \quad q = 1, 2 \quad (9)$$

where

$$[H_1] = [F_1][A_{3-q,1}]^{-1}[A_{3-q,2}],$$
$$[H_2] = [[A_{q,2}] - [A_{q,1}][A_{3-q,1}]^{-1}[A_{3-q,2}]]^{-1}$$

With the frequency sweep excitation (ω variable from zero to a selected value covering the range of n natural frequencies of the system) the results (6) to (9) are eventually graphically presented versus ω or ω^2 for the easiest curve fitting of straight lines.

Note that the model (1) takes into consideration $2n$ rotor/bering/seal system coupled modes. The vector Z contains *multimode modal coordinates,* discussed on p. xxx. Using this approach, the identification provides parameters of the coupled system, not only modal parameters of decoupled modes. The method is very effective for systems with a low number of modes (Muszynska [1986],

Muszynska *et al.* [1989b]), and is extremely useful if the knowledge on all connecting masses and stiffnesses in the system is required. If the number of modes in the chosen frequency range is not known ahead of time, the additional measurements may serve for modal correction factor calculations, as discussed by Muszynska *et al.* [1989b].

APPLICATION OF SWEEP FREQUENCY ROTATING FORCE NONSYNCHRONOUS PERTURBATION TO THE ONE-MODE ROTOR/BEARING SYSTEM. IDENTIFICATION OF WHIRL RESONANCE AND FLUID DYNAMIC FORCES

The nonsynchronous frequency swept rotating force input perturbation method has proved to be very efficient for identification of bearing and seal fluid dynamic forces. As a result of over ten years of testing and research, an improved model of fluid dynamic forces in lightly loaded bearings, in seals and fluid-handling machines, has been proposed (Muszynska [1988a]). The model was identified experimentally using the perturbation technique. A similar fluid force model was previously developed theoretically, and has existed in a simplified version in rotordynamic literature for at least 25 years (Bolotin [1963]; Black [1969, 1980]). It has not, however, been fully exploited.

The most important result of perturbation testing identification of the fluid forces was introduction of the "fluid circumferential average velocity ratio," λ, as a function of shaft eccentricity. It has replaced the assumed constant "1/2" widely used in other fluid force models.

The results of perturbation testing also, yielded, conclusions regarding modal behavior of mechanical systems with fluid interactions. It was shown that the value "$\lambda\Omega$" (fluid circumferential average angular velocity) represents (with approximation related to damping) a rotor/bearing or rotor/seal system natural frequency (Muszynska [1986]). It is associated with the specific "fluid whirl" mode of the rotor.

In the section that follows, the results of sweep frequency rotating force perturbation identification method applied to a rotor/bearing system, and the improved fluid force model in lightly loaded bearings and seals will be outlined.

The experimental rig (Fig. 7) to perform the perturbation test consisted of the main well-balanced light rotor supported in one relatively rigid bronze bushing bearing, and one oil-lubricated bearing. The main mass of the rotor was concentrated at the journal. An auxiliary light rotor was connected concentrically with the previous one through a pivoting rolling element bearing mounted inside the journal (Fig. 2b). The main rotor was rotating at a selected constant rotative speed. The auxiliary rotor carrying a light disk with a controlled unbalance weight was driven by a separate electric motor in the sweep frequency fashion. The unbalance provided the excitation force to the main rotor. The force phase was controlled by a Keyphasor®, once-per-turn marker transducer. The main rotor response was measured by two displacement transducers mounted in $X\,Y$ configuration at the lubricated bearing. The eccentricity of the journal inside the bearing was adjustable by using additional radial springs. In the "oil whirl resonance" experiment the journal initial eccentricity was zero, so the rotor forced X and Y responses were matching. The lubricant, $T10$ oil, was fed to the bearing by a supply system with controlled inlet and ambient outlet oil pressure. Four symmetrically situated radial channels, and a circumferential groove evenly distributed

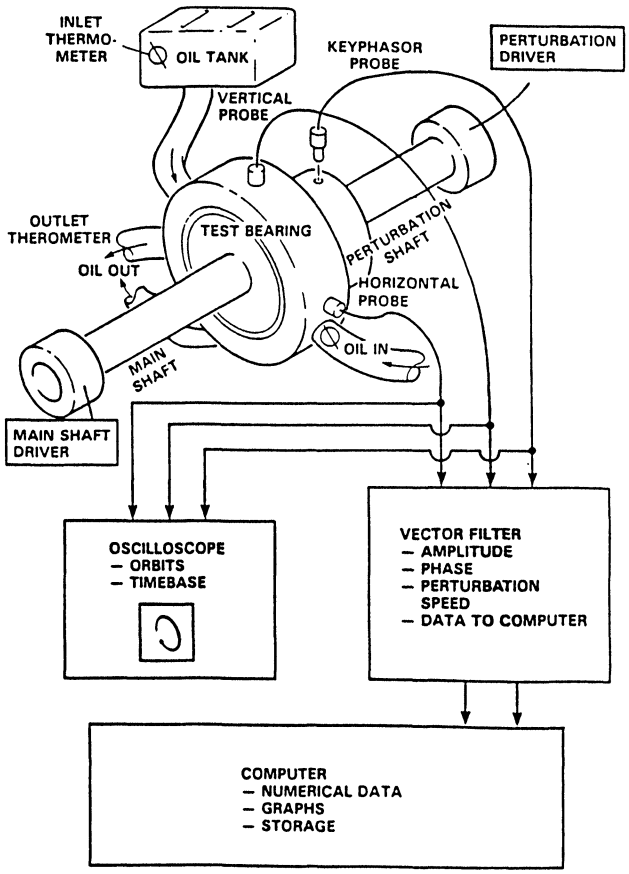

FIGURE 7 Perturbation testing rig for fluid dynamic force identification.

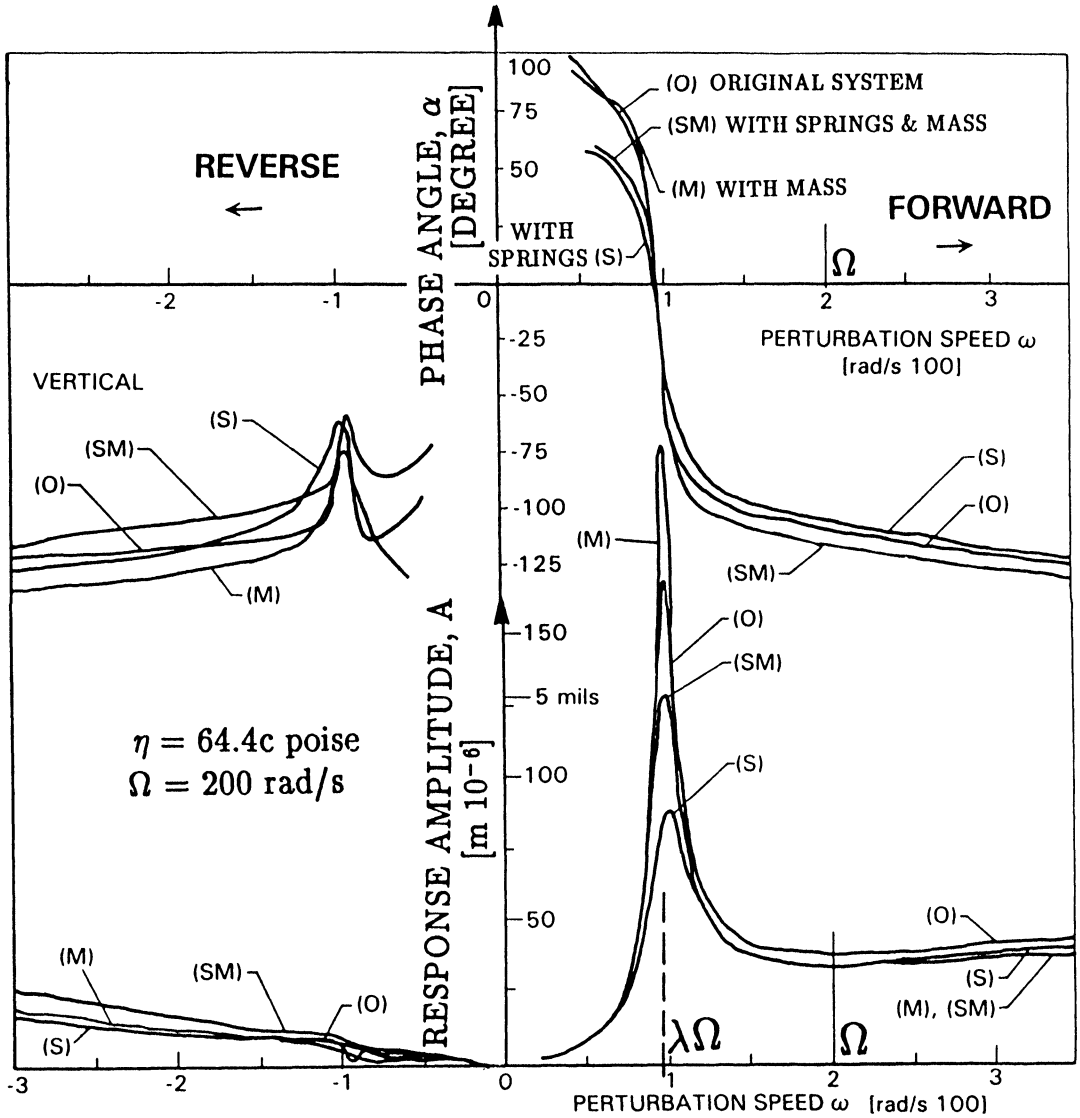

FIGURE 8 Typical plots of phase and amplitude of rotor response to forward and reverse nonsynchronous perturbation versus perturbation speed (0 = original rotor/bearing system, S = added springs, M = added rotor mass, SM = added springs and mass). Oil whirl resonance occurs at frequency close to $\Omega/2$, identified as $\lambda\Omega$ (Ω = constant rotative speed). Increase of the system mass causes an increase of the oil whirl resonant response amplitude, as margin of stability is reduced (Bently et al. [1982b]; Muszynska et al. [1990]).

the oil inside the bearing. The oil temperature was maintained constant. Both electric motors were equipped with speed control devices.

The data acquisition system consisted of the vector filter and computer. The rotor responses were continuously monitored on the oscilloscope and spectrum analyzer. The results of perturbation testing brought the following conclusions:

Fluid whirl resonance frequency. The journal X and Y responses filtered to the perturbation frequency ω, and displayed in the Bode format (Figs. 8 and 9) exhibit resonances at forward perturbation frequency equal nearly half of the constant rotative speed Ω. More precisely, the resonance occurs at $\omega \approx \lambda\Omega$ (Muszynska [1986]). At this perturbation frequency the response amplitude has a peak, and the phase angle sharply changes values through zero degree. This yields the conclusion that $\lambda\Omega$ is the rotor/bearing system natural frequency (Muszynska [1986]). This resonance has a "quadrature" character, and became known as "oil whirl resonance" or, more generally, as "fluid whirl resonance." Such resonance does not occur for the reverse perturbation.

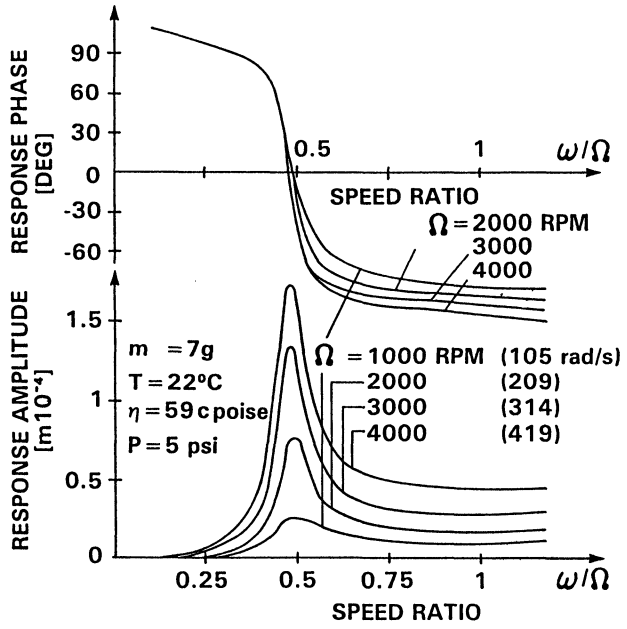

FIGURE 9 Phase and amplitude of rotor response versus perturbation-to-rotative speed ratio for various values of rotative speeds, Ω. Increase of amplitudes with increases of Ω due to decrease of margin of stability (Bently et al. [1992a, b]; Muszynska [1986, 1990]).

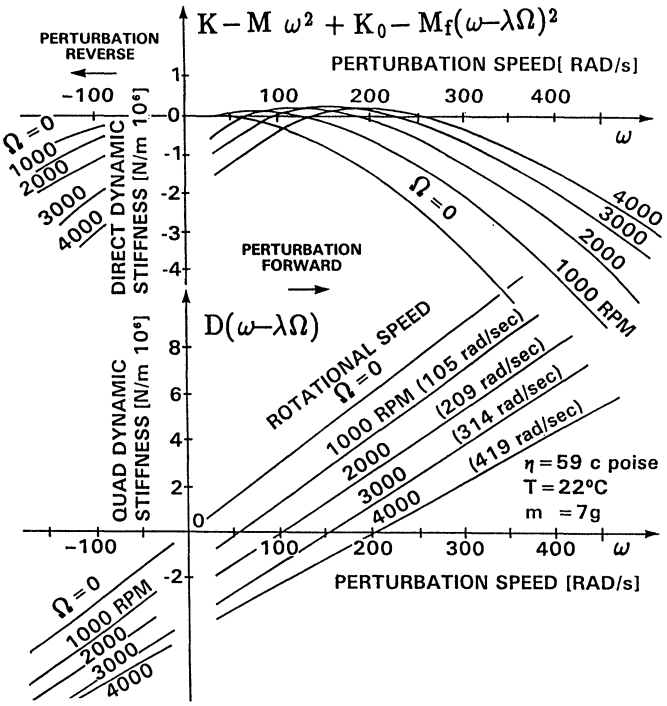

FIGURE 10 Rotor/bearing direct and quadrature dynamic stiffnesses versus perturbation speed. Identification of fluid force parameters. (Higher rotative speeds caused an increase of oil temperature, thus a decrease of fluid radial damping reflected in quadrature dynamic stiffness graphs with lower slopes) (Muszynska [1986, 1990]). K, M are rotor stiffness and mass, respectively.

Dynamic stiffness format. Using the dynamic stiffness algorithm (Eqs. (7) to (9)), the force/response data was then processed, and presented in the dynamic stiffness format. For the isotropic single complex degree of freedom system ($x + jy = z$; $j = \sqrt{-1}$) the journal lateral response was $z = A\exp[j(\omega t + \alpha)]$, where A and α are response amplitude and phase filtered to perturbation frequency ω. The Direct (DDS) and Quadrature (QDS) dynamic stiffnesses were obtained as

$$\text{DDS} = \frac{mr\omega^2}{A}\cos(\delta - \alpha),$$

$$\text{QDS} = \frac{mr\omega^2}{A}\sin(\delta - \alpha) \qquad (10)$$

where m, r, δ are the input perturbation force unbalance mass, radius, and angular orientation, respectively.

The dynamic stiffness components versus perturbation frequency are presented in Fig. 10. The direct dynamic stiffnesses are parabolas; the quadrature ones are straight lines, thus the identification of their parameters is relatively easy.

Fluid force model. The curve fitting of the dynamic stiffness components allowed identification of the fluid force model applicable for lightly loaded bearings and seals (Muszynska [1986, 1988a]; Muszynska *et al.* [1990]). The following fluid force model

$$F = [K_0 + jD(\omega - \lambda\Omega) - M_f(\omega - \lambda\Omega)^2]Ae^{j\alpha} \qquad (11)$$

was provided directly from the dynamic stiffness graphs; $\text{DDS} = K_0 - M_f(\omega - \lambda\Omega)^2$, $\text{QDS} = D(\omega - \lambda\Omega)$. (Note that the raw data in Fig. 10 also contain, the mechanical system parameters K and M which were subtracted, and do not appear in the fluid force model (11).)

The differential form of the fluid force model in coordinates rotating with angular velocity $\lambda\Omega$ is (Muszynska [1988a]):

$$F = K_0 z_r + D\dot{z}_r + M_f\ddot{z}_r \qquad z = x + jy = z_r e^{j\lambda\Omega t} \qquad (12)$$

In stationary coordinates $z = x + jy$ the fluid force model becomes:

$$F = K_0 z + D(\dot{z} - j\lambda\Omega z) + M_f(\ddot{z} - 2j\lambda\Omega\dot{z} - \lambda^2\Omega^2 z) \qquad (13)$$

In Eqs. (11) to (13) K_0, D, and M_f are fluid radial stiffness, radial damping, and inertia effect, respectively, all of

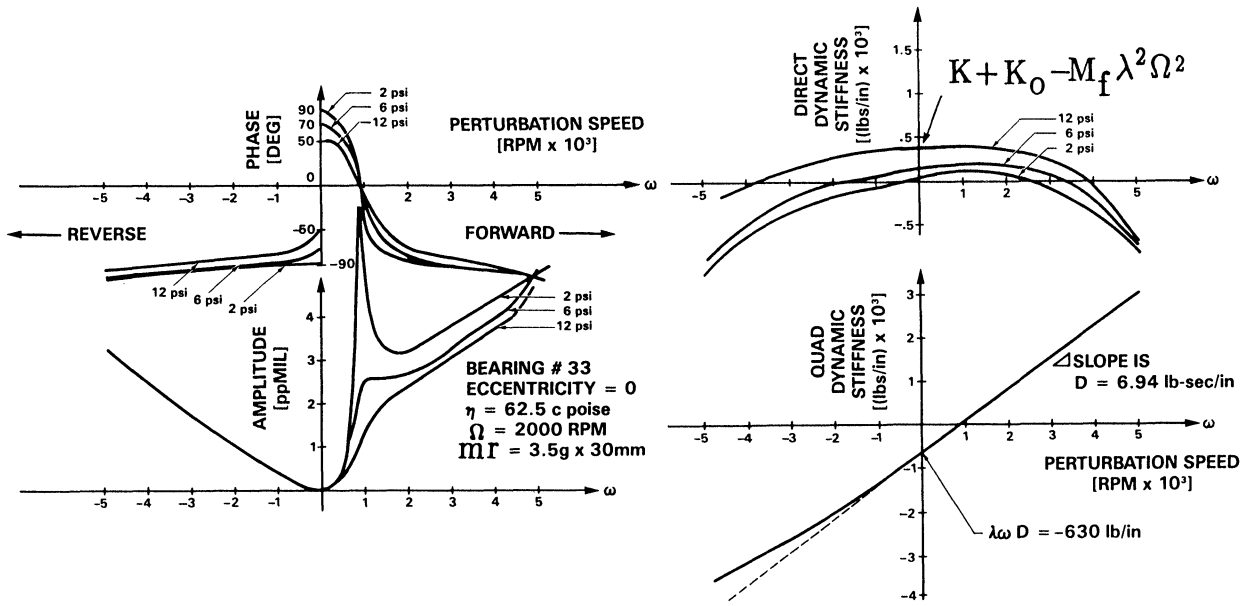

FIGURE 11 Phase, amplitude, and dynamic stiffnesses versus perturbation speed for several values of oil pressure: an increase of fluid radial stiffness and, consequently, of the stability margin for higher pressure (Muszynska [1986, 1990]).

them at zero eccentricity of the shaft inside the bearing or seal.

The most dominant parameter of the fluid force is the fluid radial damping D. The total quadrature dynamic stiffness value is usually much higher than the direct dynamic stiffness. The rotational character of the fluid radial damping force results in an appearance of the component known as the "cross stiffness," "K_{xy}." The results of perturbation testing proved that this term is directly proportional to the damping, D, and to the fluid circumferential average velocity ratio, λ. The latter provides an efficient way to control the value of this "cross stiffness" term, thus to control the stability of the rotor/bearing/seal system (Bently *et al.* [1988], Muszynska *et al.* [1989a]).

Fluid whirl mode. When the rotor is rigidly supported at one end, as it was in the case of the described experiment, the fluid whirl mode is conical. The shaft vibrates in phase with the journal, as a rigid body (Muszynska [1986, 1988c]).

Fluid force parameters as functions of various factors. Variations of the rotative speed, including zero speed (squeeze film damper), yielded the most important conclusion regarding rotational character of the fluid dynamic force, and provided some insight into the fluid inertia effect (Figs. 9 and 10). Variations of the lubricant pressure and temperature allowed to identify the influence of these factors on the separate parameters of the fluid force model. As it is shown in Fig. 11, an increasing lubricant pressure increases the fluid radial stiffness, K_0.

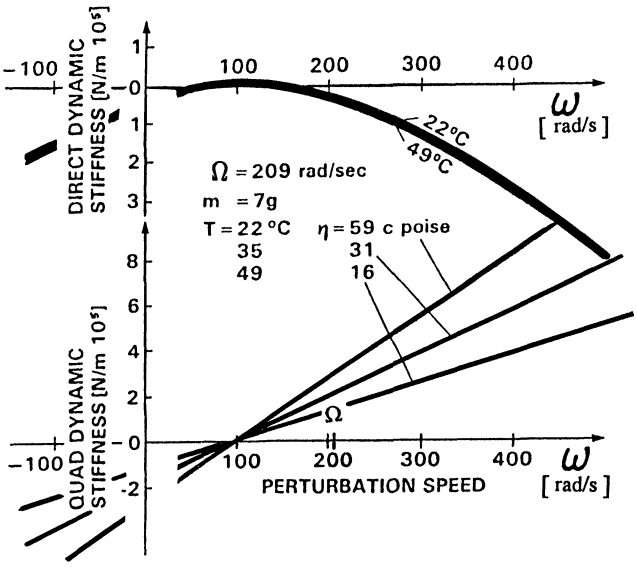

FIGURE 12 Rotor bearing direct and quadrature dynamic stiffnesses versus perturbation speed for three values of oil temperature. Results indicate modifications of fluid radial damping, D (Bently *et al.* [1982b]; Muszynska [1986]).

An increased lubricant temperature (decreasing viscosity) causes a decrease of the fluid radial damping (Fig. 12). Variations of the perturbation force amplitude provided results which helped to identify nonlinearities of the fluid radial stiffness and damping versus eccentricity (Figs. 13, 14, and 15).

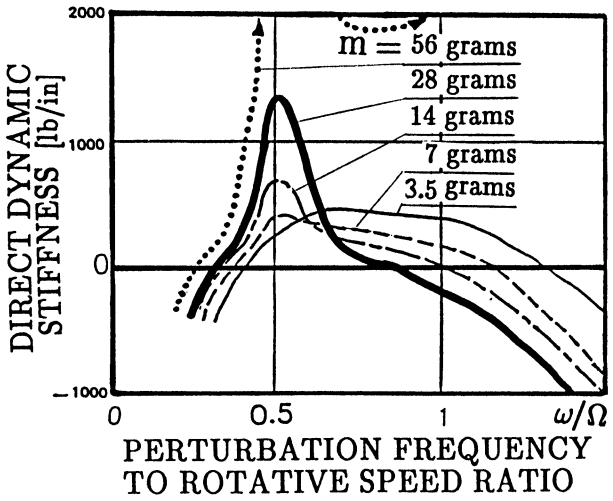

FIGURE 13 Direct dynamic stiffnesses with nonlinear effects (perturbation by increasing perturbation force magnitude, m = controlled input unbalance weight mass) (Bently *et al.* [1985a, 1986a]; Muszynska *et al.* [1990]).

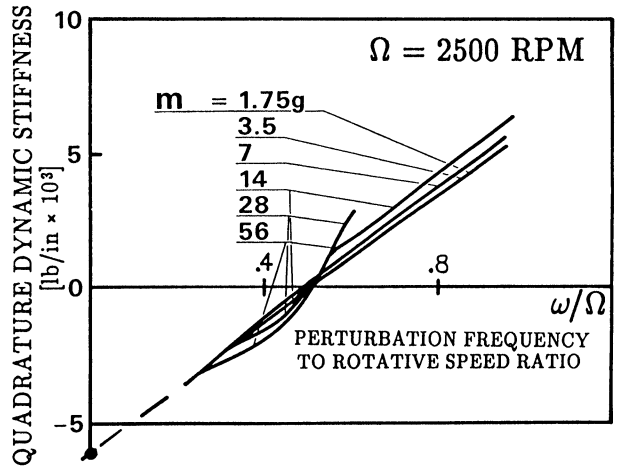

FIGURE 14 Quadrature dynamic stiffness with nonlinear effects (perturbation by increasing perturbation force magnitude, m = controlled input unbalance weight mass) (Bently *et al.* [1985a, 1986a]; Muszynska, *et al.* [1990]).

COMPARISION OF THE RESULTS OF PERTURBATION TESTING USING ROTATING FORCE INPUT AND ROTATING DISPLACEMENT INPUT

There are two main perturbation techniques of nonsynchronous one-mode testing used for identification of fluid force models in rotor/bearing, rotor/seal systems, and in fluid handling machines (mainly pumps). The basic advantage of these methods is the rotational character of the input function, in forward or reverse direction (the same or opposite to rotor rotation). This allows for independent identification of forward and backward modes of the rotating system. The two perturbation techniques differ by the input/output functions (Figs. 2 and 4). They are follows:

$$\text{FORCE: } Fe^{j\omega t} \longrightarrow \boxed{\bar{H}(\omega) = \frac{1}{\kappa(\omega)}} \longrightarrow \text{DISPLACEMENT: } Ae^{j(\omega t+\alpha)}$$

$$\text{DISPLACEMENT: } Ae^{j\omega t} \longrightarrow \boxed{\kappa(\omega) = \frac{1}{\bar{H}(\omega)}} \longrightarrow \text{FORCE: } (F_r + jF_t)e^{j\omega t}$$

where A is rotor displacement amplitude, α is rotor response phase (also $\alpha = \arctan(-F_t/F_r)$), ω is rotor perturbation (excitation) precessional frequency (usually varying from zero to some $\omega_{\max}$), and F_r, F_t are radial and tangential forces, acting on the rotor. These forces are obtained by integrating the fluid pressure or measuring forces outside an elastically supported seal or bearing; F is the input force amplitude.

In both techniques the objective is identification of the transfer function of the system. More precisely, the functions sought are $\kappa(\omega)$ = Complex dynamic stiffness, or $\bar{H}(\omega) = \frac{1}{\kappa(\omega)}$ = Transfer function = Complex dynamic compliance of the system. The result most often obtained from either technique is the complex dynamic stiffness:

$$\kappa(\omega) = \frac{F_r + jF_t}{A} \quad \text{when inputting displacement} \tag{14}$$

$$\kappa(\omega) = \frac{F}{A}e^{-j\alpha} \quad \text{when inputting force} \tag{15}$$

The complex dynamic stiffness components for both techniques are as follows:

$$\text{Direct dynamic stiffness} \equiv \text{DDS} = \frac{F_r}{A} = \frac{F\cos\alpha}{A} \tag{16}$$

$$\text{Quadrature dynamic stiffness} \equiv \text{QDS} = \frac{F_t}{A} = -\frac{F\sin\alpha}{A} \tag{17}$$

By limiting the input to a circular periodic function, both methodologies should yield *exactly* the same results, *provided* that the system is linear, and the instrumentation allows for comparable signal-to-noise ratios.

Both techniques are known in mechanics as "force excitation" and "kinematic excitation," respectively. They both serve well for identification of the lowest mode generalized (modal) parameters of the system.

Figures 8, 9, 10, 16 and 17 illustrate the basic results obtained by various researchers who used either of

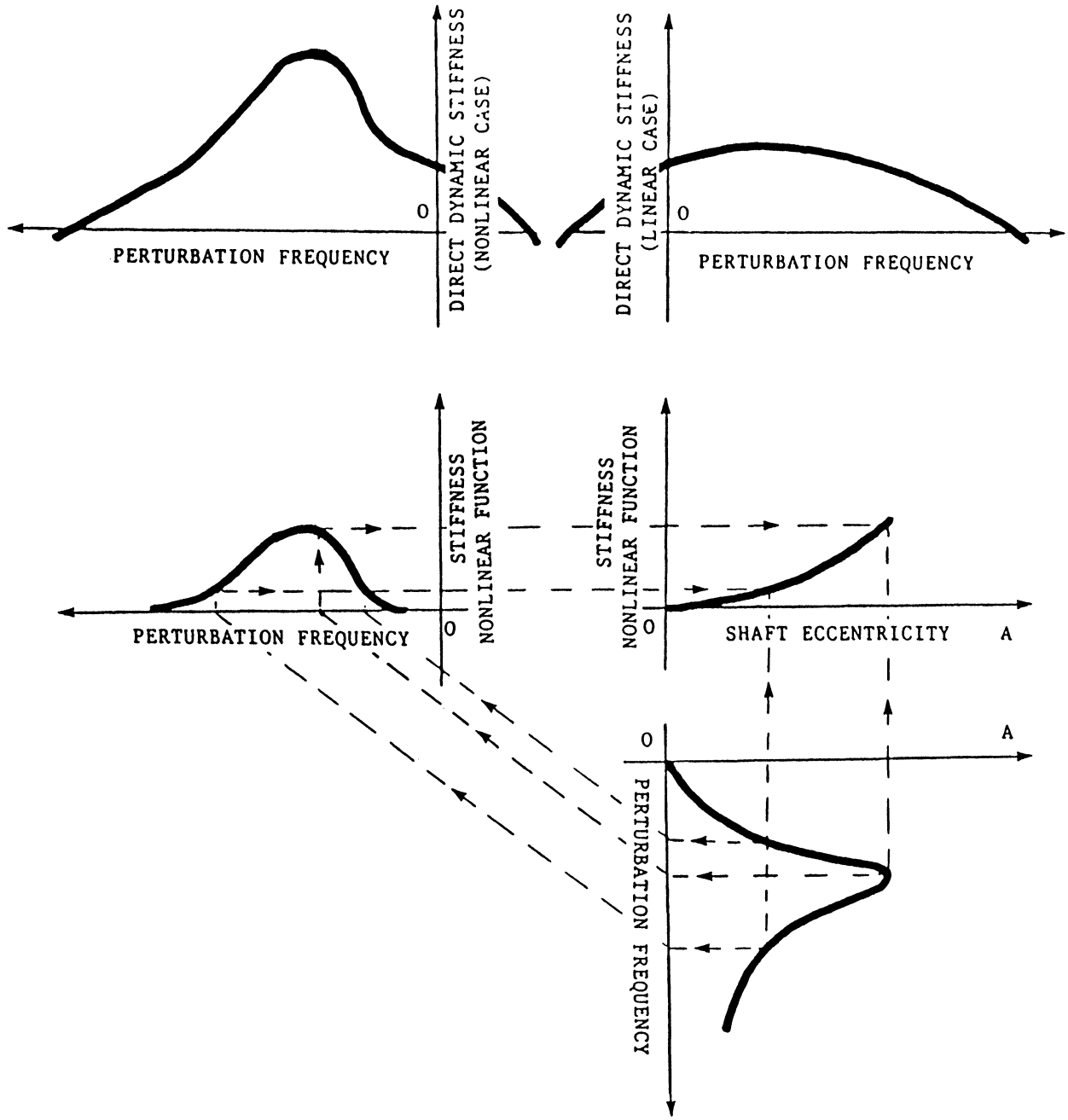

FIGURE 15 Identification of fluid radial stiffness nonlinearity (Muszynska *et al.* [1990]). Stiffness nonlinear function results from subtraction of dynamic stiffnesses for nonlinear and linear cases.

the nonsynchronous perturbation techniques. Following Eqs. (14) and (15), the dynamic stiffness graphs versus perturbation frequency (Figs. 10 and 17) are similar for both techniques. The response vectors versus perturbation frequency are presented in Figs. 8, 9 and 16, in the form of Bode plots. Note that, in the technique which uses force input, the displacement response vector to forward perturbation has a form characteristic for responses of a one-mode system to a periodic excitation with sweep frequency (Figs. 8 and 9). The occurrence of a resonance is obvious. The peak amplitudes may become very high if the shaft rotative speed approaches the $1/\lambda$ value of the rotor "mechanical" natural frequency, corresponding to its first bending mode (λ is the fluid circumferential average

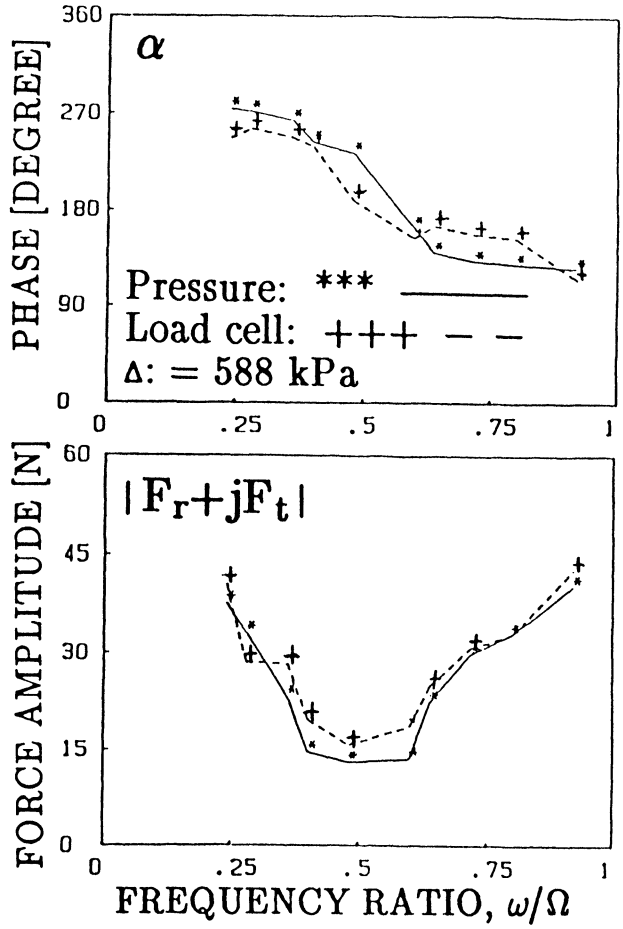

FIGURE 16 Force response phase and amplitude versus perturbation frequency (perturbation by displacement). Courtesy of T. Iwatsubo [1988].

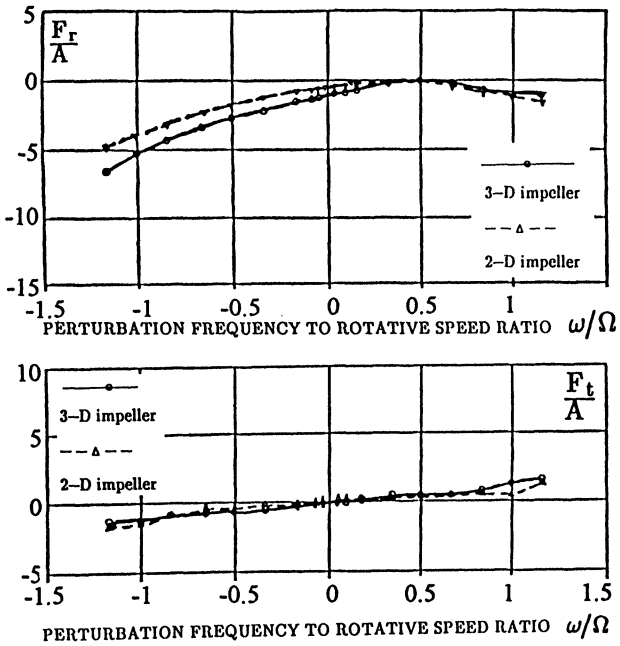

FIGURE 17 Direct and quadrature dynamic stiffness versus perturbation frequency for the system with input = circular displacement, and output = force (see Eq. [14]). Courtesy of H. Ohashi [1988].

velocity ratio), as discussed by Muszynska [1986, 1990]. In fact, instability occurs when both direct and quadrature dynamic stiffnesses are nullified at the same frequency. In comparison to the response of a classical mechanical system, the response phase is, however, ahead of the input force. This indicates the "quadrature" nature of this particular resonant phenomenon. The resonant frequency has been identified as $\lambda\Omega$. (In machinery it was sometimes called "bearing resonance."). The occurrence of the resonance suggests that $\lambda\Omega$ represents one of the system natural frequencies. This natural frequency is generated purely by the fluid/solid interaction. The rotating shaft drags the fluid into circumferential motion, generating the fluid rotating forces which act on the shaft in a feedback loop. This fluid-related quadrature resonance was documented by Stone & Underwood in 1947, and again by Hull in 1955, but these excellent works were not immediately pursued.

By inputting a constant circular displacement, and measuring the output in terms of forces, the accuracy of the results is lower (mainly due to poor phase resolution), and there is no clear physical interpretation of the results. The plot of force response amplitude versus perturbation frequency has an "anti-resonance" shape, a concave curve, like a mirror image of displacement response amplitude versus frequency (Fig. 16). The phase is the same in both techniques. It is obvious, because by definition, the phase represents the angle between the input vector and output vector, independently of the nature of the input and output functions. Note that the dip point of the response force amplitude and phase drop occur around one half of the rotative speed, i.e., the fluid circumferential average velocity ratio λ is equal to about one half. The notion of the "force resonance," or rather "anti-resonance," is not known in mechanics. That is why the researchers who have used the input force methodology, and adopted direct physical interpretation of the results, have been more fortunate than those who use forces as outputs.

Note the advantage of the circular perturbation, as opposed to unilateral perturbation, in impulse testing. The results of forward perturbation (rotation and precession in the same direction), and backward perturbation (opposed direction) are significantly different (Fig. 8). The resonance occurs only for the forward perturbation, that is,

the "quadrature" natural frequency $\lambda\Omega$ of the system has only the plus sign (classical "direct" natural frequencies governed by stiffness and mass have + and − signs).

ANTISWIRL SEAL TESTING

The sweep frequency rotating force nonsynchronous perturbation method was applied to identify the fluid force parameters in antiswirl seals equipped with radial and tangential inlet ports (Grant [1991]). The results provide clear effects of the input flow pattern on fluid force components. Water was used for series of experiments. Figure 18 illustrates an example of the data presented in terms of dynamic stiffness components for the seal input flow through radial or antiswirl ports for three rotative speeds. Based on this type of data, the identified fluid force parameters, namely, circumferential average velocity ratio λ, radial stiffness, and damping reduced from approximately 70 runs covering the range from 3 to 80 psi water pressure, are presented in Figure 19. The graphs clearly show general trends of these parameters for radial and antiswirl inlets (Muszynska *et al.* [1992]).

Figure 20 illustrates fluid circumferential average velocity ratio versus anti-swirl port pressure drop for several cases of mixed radial and tangential inlets. As seen in Figures 19 and 20, the antiswirl input fluid injection in the direction opposite to shaft rotation makes dramatic changes in the fluid circumferential average velocity ratio values, considerably lowering them, and improving rotor stability features.

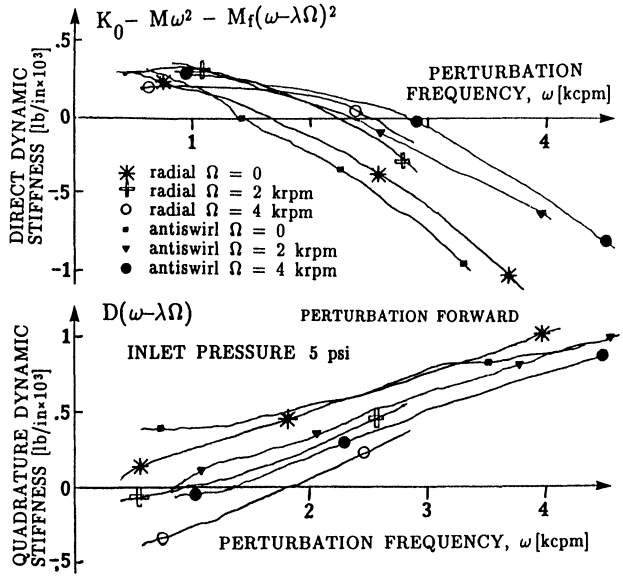

FIGURE 18 Direct and quadrature dynamic stiffnesses versus perturbation frequency of the seal with either radial or antiswirl inlet ports (Grant [1991]; Muszynska *et al.* [1992]).

ROTOR/BEARING SYSTEM IDENTIFICATION COVERING WHIRL AND WHIP MODES

In the tests for identification of the fluid whirl resonance, the main rotor was deliberately rigid and light, so that its first natural frequency of the bending mode (conventionally called here "whip") was well above the range of perturbation frequencies. The next series of tests concerned the rotor/bearing system, covering both whirl and whip modes. The main rotor was made more elastic, and a heavy disk was mounted at rotor mid-span (Fig. 21). The main rotor first natural frequency became much lower, and placed in the range of the applied perturbation frequencies. Since more modes were involved, the test required additional data. Perturbation, therefore, was applied either at the journal (as previously), or at the rotor disk (using an unbalanced, pulley-driven spinner). Each time, the response data was collected from XY proximity transducers mounted at the bearing, and at the disk. Following the identification algorithm (7) to (9), the 2×2 matrix of complex dynamic stiffness components was identified. The results are presented in the form of Bode plot matrices from the experimental data, as well as from calculated analytical data based on the identified parameters of the system. The system model (Fig. 22) is as follows (Bently *et al.* [1985c]):

$$M_d\ddot{z}_d + D_s\dot{z}_d + (K_1 + K_2)z_d - K_2\sigma z_b = \begin{cases} F_d e^{j\omega t} & \text{for the first test} \\ 0 & \text{for the second test} \end{cases}$$

$$M_b\ddot{z}_b + M_f(\ddot{z}_b - 2j\lambda\Omega\dot{z}_b - \lambda^2\Omega^2 z_b) + D(\dot{z}_b - j\lambda\Omega z_b) + (K_0 + K_3)z_b + K_2(\sigma z_b - z_d) = \begin{cases} 0 & \text{for the first test} \\ F_b e^{j\omega t} & \text{for the second test} \end{cases} \quad (18)$$

where M_d, M_b are disk and journal modal masses correspondingly, K_1 and K_2 are the main shaft partial modal stiffnesses, σ is modal correction factor, K_3 is the external supporting spring stiffness, D_s is rotor external modal

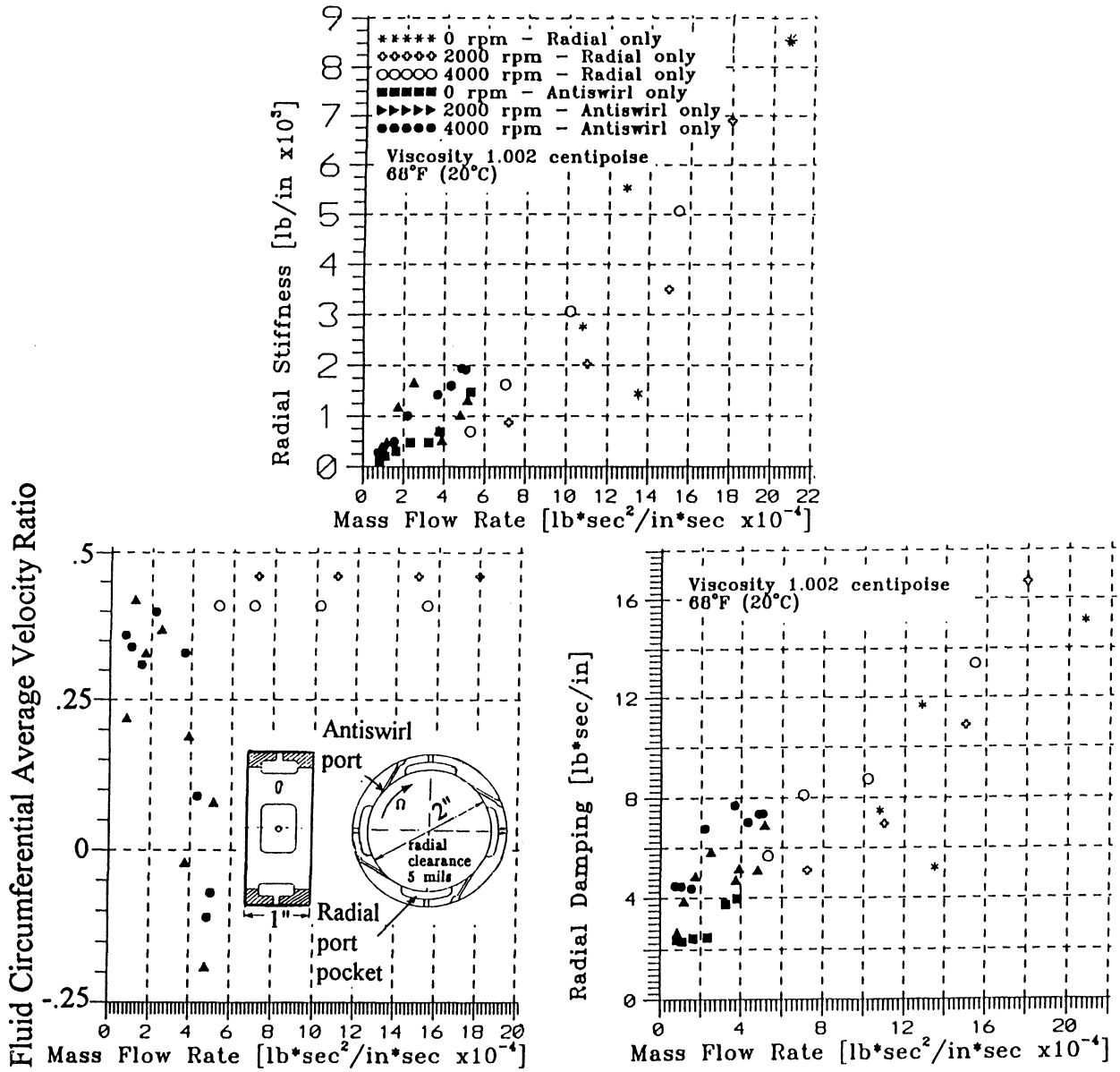

FIGURE 19 Identified fluid radial stiffness (K_0), fluid circumferential average velocity ratio (λ), and damping (D) of the antiswirl seal versus measured mass flow rate (Grant [1991]; Muszynska *et al.* [1992]).

viscous damping, M_f, D, K_0 are, as previously, the fluid force parameters, F_d and F_b are perturbation force amplitudes ($F_d = m_{pd} r\omega^2$, $F_b = m_{pb} r\omega^2$). The results presented in the form of Bode plot matrix exhibit two resonant ranges: the whirl resonance at lower perturbation frequency discussed on p. xxx, and the "whip" resonance corresponding to the rotor first bending mode. Using the dynamic stiffness algorithm (Eqs. (7) to (9)), the system parameters were identified. As it can be seen from the corresponding experimental (Fig. 23) and analytical (Fig. 24) results, the identification process provided very good agreement, and proved the model adequacy.

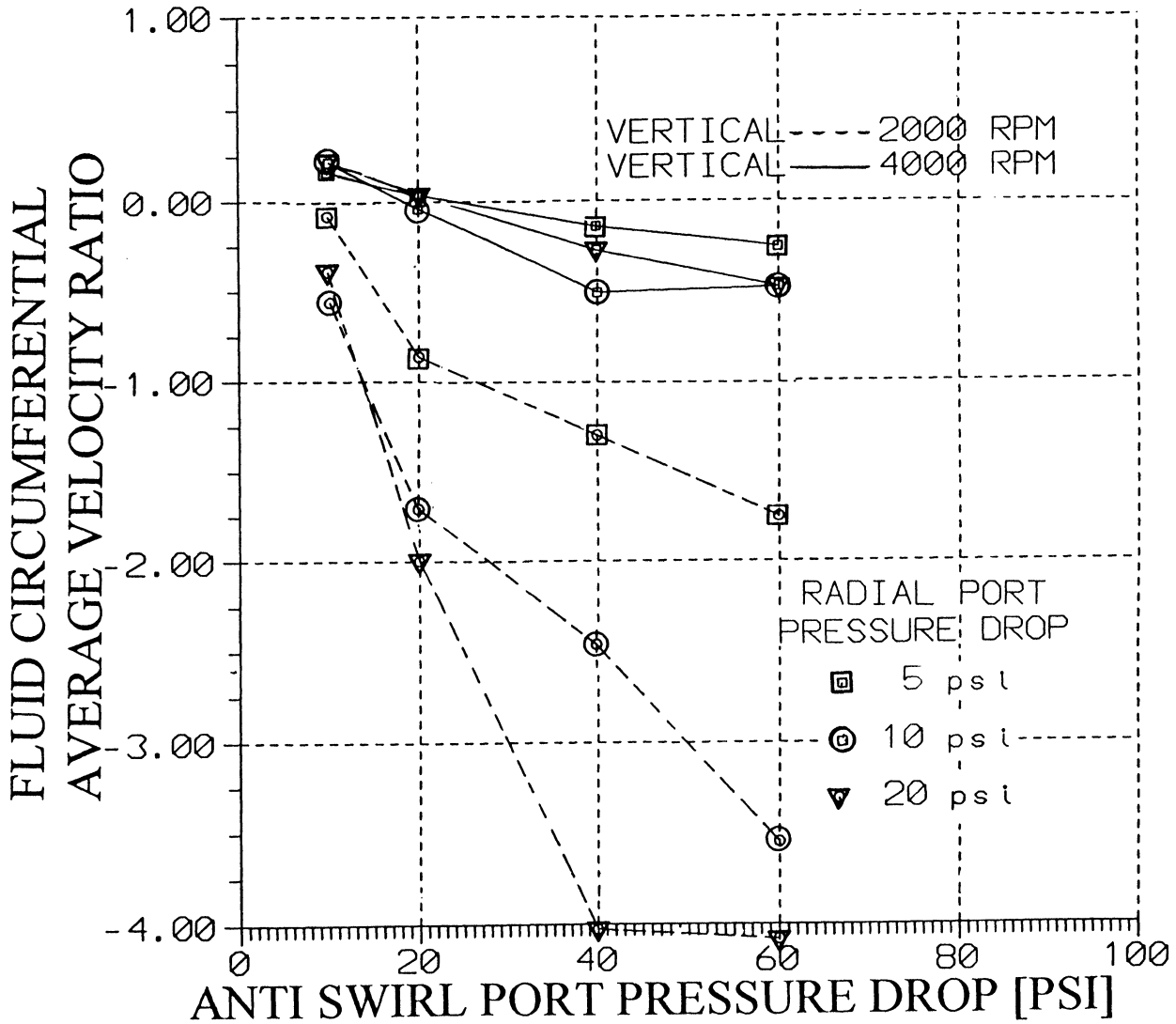

FIGURE 20 Fluid circumferential average velocity ratio (λ) versus antiswirl port pressure drop.

SQUEEZE FILM PERTURBATION TESTS, STEADY-STATE LOAD TESTS, AND IMPULSE TESTS OF ROTOR/BEARING SYSTEMS

Squeeze film tests of bearings are circular force perturbation tests of a rotor at rest, and usually performed at zero initial journal eccentricity of a rotor, so the results are isotropic. The fluid force (13) for the squeeze film tests does not contain terms depending on Ω. When the dynamic stiffness components of the tested bearing are plotted versus perturbation frequency (QDS), or versus perturbation frequency squared (DDS), the parameters D, K_0 and M_f can easily be identified from resulting straight lines. Figure 25 presents Direct Dynamic Stiffness of a bearing fluid obtained from the squeeze film test. The data exhibit very high fluid inertia effect, practically independent from fluid inlet pressure.

Steady-state load test of a rotor/bearing system is accomplished by applying a constant radial force to the rotating journal, and measuring the journal displacements in two orthogonal directions. These displacements are presented in the eccentricity ratio polar format for several values of the rotative speeds and input radial forces (from 2 to 15 lbs) (Fig. 26). The journal displacements exhibit two distinctly different patterns of behavior. In the low eccentricity range, the dominant component of the fluid force has a quadrature nature: displacement is almost

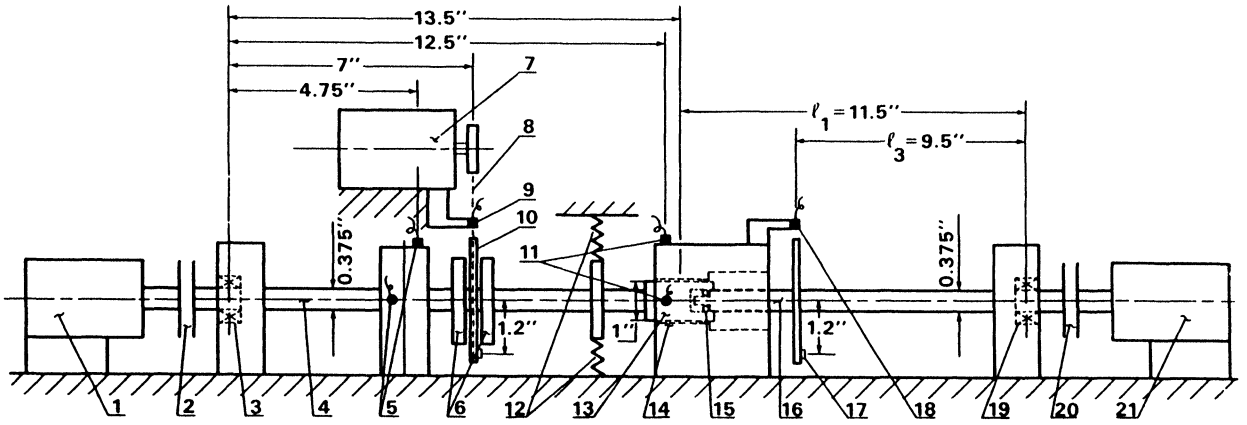

FIGURE 21 Test rig (Bently *et al.* [1985c]). (1) main motor; (2) elastic coupling; (3) rigid pivoting bearing; (4) main shaft, (5) disk XY noncontacting probes; (6) main rotor disks; (7) disk perturbation motor; (8) perturbation driving system; (9) Keyphasor® probe; (10) disk with perturbation unbalance; (11) bearing XY noncontacting probes; (12) rotor weight balancing springs; (13) main rotor journal; (14) oil-lubricated bearing with radial clearance 25 μm; (15) pivoting bearing connecting auxiliary shaft to the journal; (16) auxiliary perturbing shaft; (17) disk with perturbation unbalance; (18) Keyphasor® probe; (19) rigid bearing; (20) elastic coupling; (21) perturbation motor.

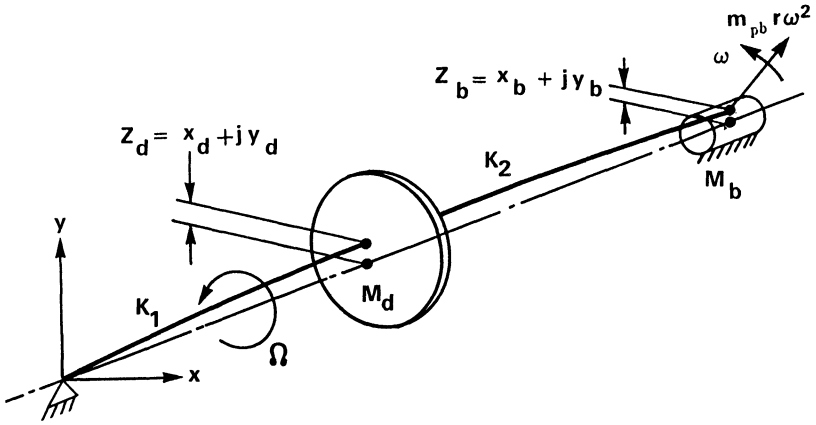

FIGURE 22 Model of the isotropic rotor/bearing system, taking into account two complex modes.

perpendicular to the applied force, that is, the tangential (quadrature) component of the fluid force, $D\lambda\Omega$, is dominant. For a high rotative speed the angle between the input force and journal response is even larger than 90°, which indicates a high fluid inertia effect opposing the fluid film radial stiffness* (Bently *et al.* [1985a]).

In order to identify the fluid force parameters, the input force vector was divided by the response vector, split into collinear and perpendicular to the input force components, and presented versus eccentricity ratio (Fig. 27). While the quadrature components identified as λD (rotative speed eliminated) exhibit classical, quite regular form, the fluid film dynamic stiffness in the direction of load, namely, $K - M_f\lambda^2\Omega^2$ confirms the existence of the strong fluid inertia effects, and exhibits two distinct patterns of behavior characteristic for the low and high eccentricities.

A similar steady-state load test was performed on a low-pressure oil bearing (Fig. 28). While the fluid inertia effect was smaller, similar behavior patterns in the two ranges of eccentricity were observed. In both cases (Figs. 26 and 28)

*The fluid dynamic force for this test is $F = (K_0 - Dj\lambda\Omega - M_f\lambda^2\Omega^2)z$ (see Eq. (13)); the force balance is $F = Pe^{j\gamma}$ where P, γ are amplitude and angular orientation of the input constant radial force. By measuring "z," the fluid force can be identified.

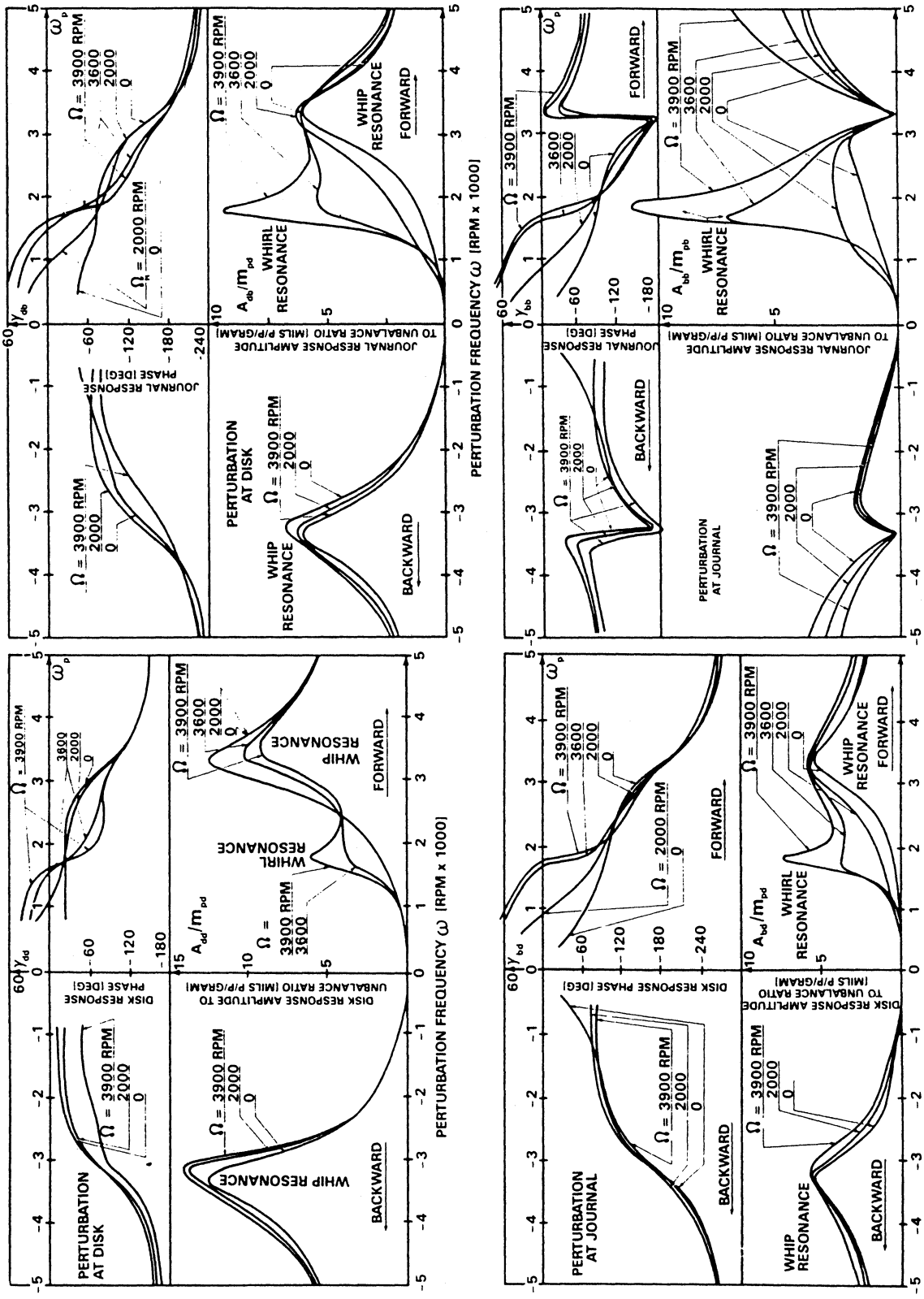

FIGURE 23 Experimentally obtained matrix of rotor/bearing system response phases and amplitudes versus perturbation frequency. (a) and (b) represent results of perturbation at the disk; (c) and (d) represent results of perturbation at the journal (Bently *et al.* [1985c], Muszynska [1986]).

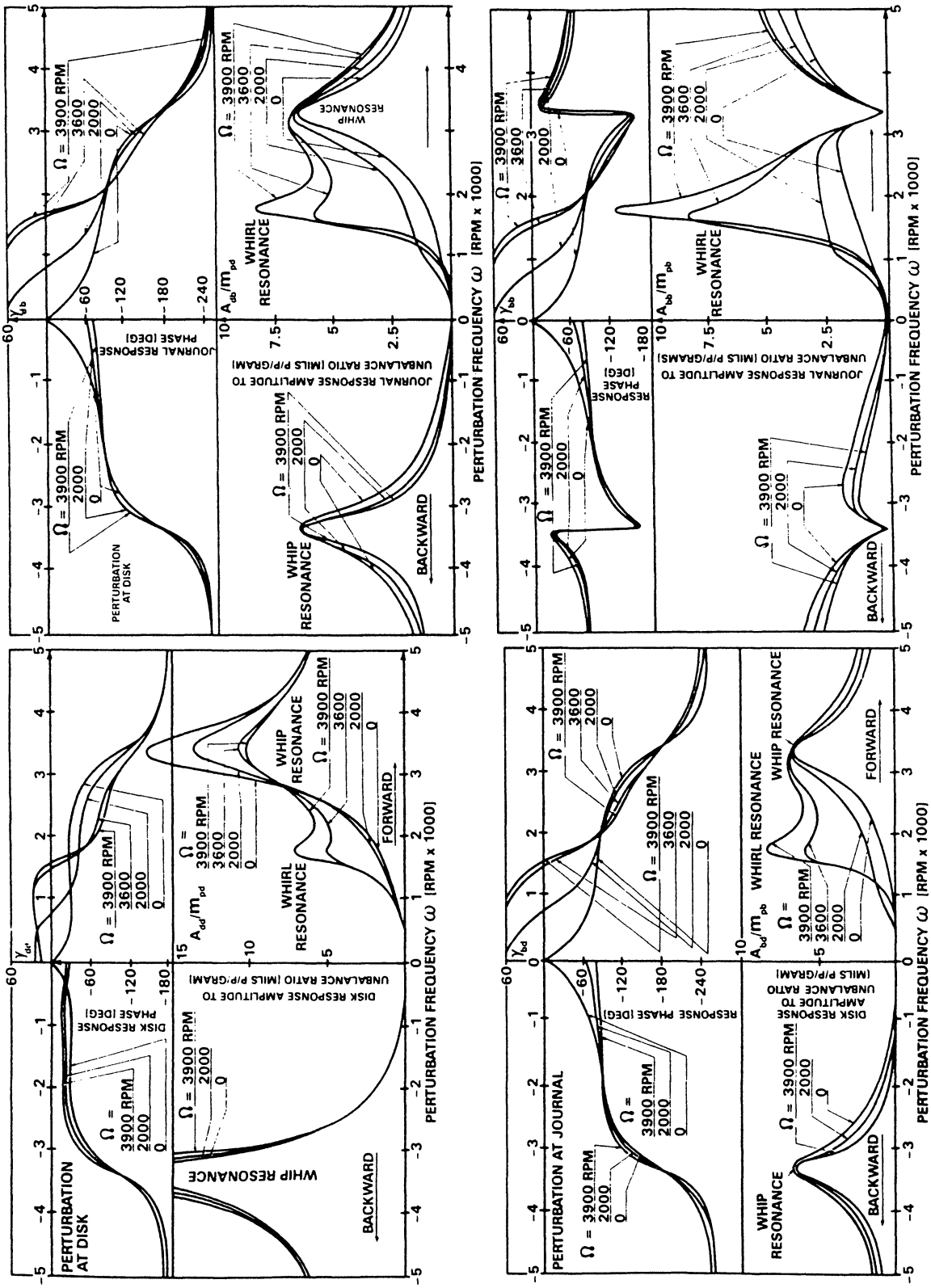

FIGURE 24 Analytically calculated rotor/bearing system response phases and amplitudes based on Eqs. (18), and using parameters identified from the experiment (Bently *et al.* [1985c]; Muszynska [1986]). Compare with Figure 23.

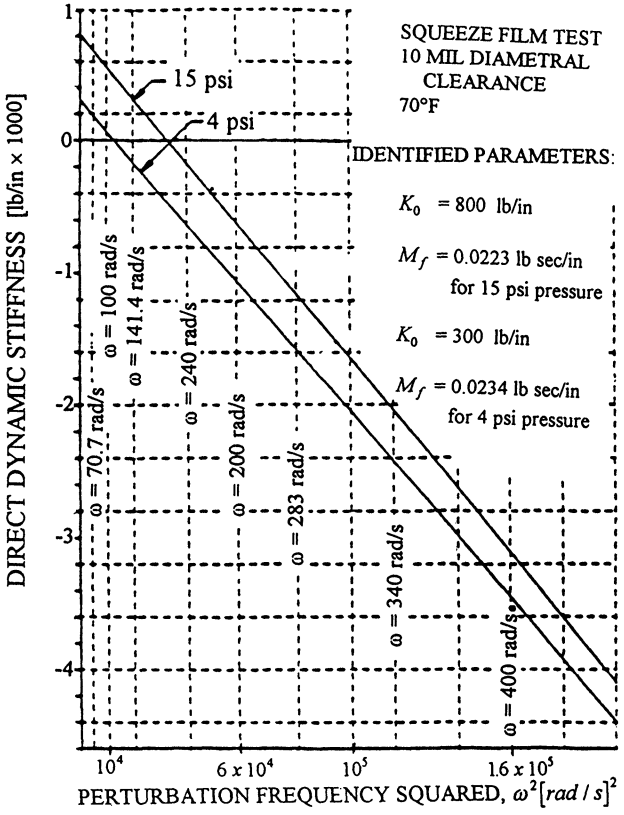

FIGURE 25 Direct Dynamic Stiffness of a cylindrical bearing (l/d = 0.74) obtained from the squeeze film test (Bently *et al.* [1985a]).

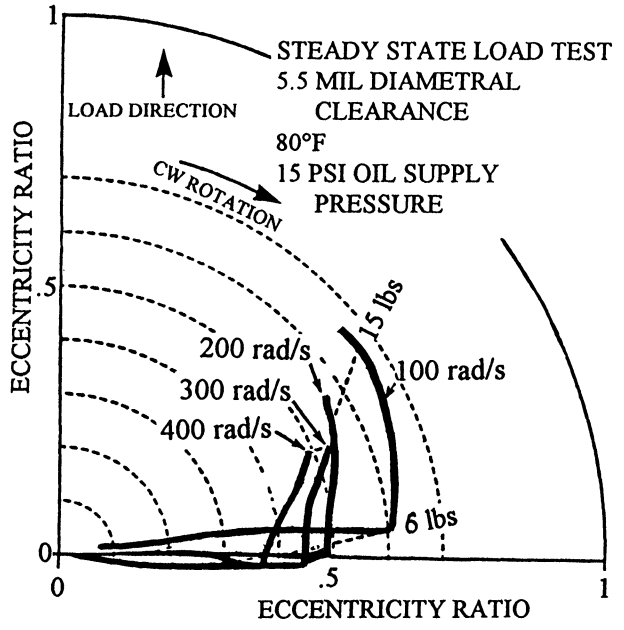

FIGURE 26 Pressurized cylindrical bearing journal centerline response to constant vertical force for several values of rotative speeds and input force amplitudes (Bently *et al.* [1985a]).

the quadrature stiffness dominance ceases at lower eccentricity, when rotative speed is higher.

Different dynamic behavior of the journal at low and high eccentricities corresponds to significant changes in the flow patterns: at low eccentricities the flow pattern is predominantly circumferential, due to shaft rotation, and $D\lambda\Omega > K_0$. In this range the fluid force model (12), (13) is adequate. At high eccentricities the circumferential flow is suppressed by increasing axial flow pattern, $D\lambda\Omega < K_0$.

The changes of flow patterns were eventually confirmed by impulse testing. The shaft (rotating at a constant speed in a fluid-lubricated bearing at one end and in a rigid bearing bushing on the other end) was impacted by a calibrated hammer. The XY proximity probes mounted in the bearing, observed the journal transient responses. The data acquisition and processing system recorded the frequencies of the transient responses at different original journal eccentricities. These frequencies were then divided by corresponding constant rotative speeds. The results identified as fluid circumferential average velocity ratio (λ) are presented in Figure 29 for two different bearings.

The circumferential pattern of flow at low eccentricity is evident, which produces the rotor/bearing system natural frequency $\lambda\Omega$, which was previously discovered by nonsynchronous perturbation testing. The average circumferential velocity first slightly decreases with increasing eccentricity, then collapses at higher eccentricity. Interesting enough is that when the rotative speed is high, the range of low eccentricity where circumferential flow pattern is present appears narrower than for low rotative speeds. The similar result regarding direct stiffness behavior (see Fig. 27) was obtained from the static load test.

PARAMETER IDENTIFICATION OF A ROTOR WITH STRONG GYROSCOPIC EFFECT

The overhung isotropic rotor rig schematically shown in Figure 30 was used for identification of rotor parameters by applying lateral nonsynchronous forward and backward circular force perturbation testing (Bently *et al.* [1986b]). The rotor natural frequencies were identified as resonant frequencies of rotor responses filtered to perturbation frequency. The sequence of polar plots of rotor vertical and axial responses for the forward and backward perturbation is shown in Figure 31. Figure 32 presents the rotor natural frequencies as functions of rotative speed, that is the well-known relationship for rotors with strong gyroscopic effect.

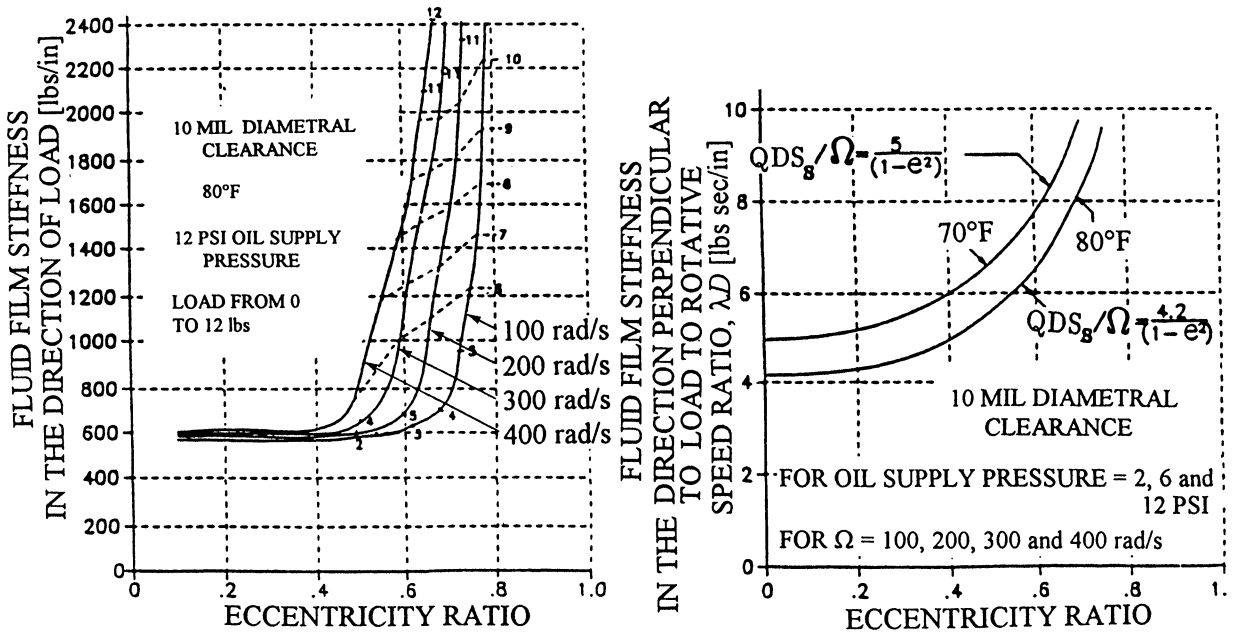

FIGURE 27 Cylindrical pressurized bearing ($\ell/d = 0.74$) fluid film dynamic stiffness components versus eccentricity ratio (Bently *et al.* [1985a]).

Since the simple two-mode model of the rotor contains at least eight parameters, the lateral perturbation only was not sufficient to identify all of them, without additional assumptions. Assuming, however, the disk transverse moment of inertia is known, the remaining parameters were identified (Bently *et al.* [1986b]).

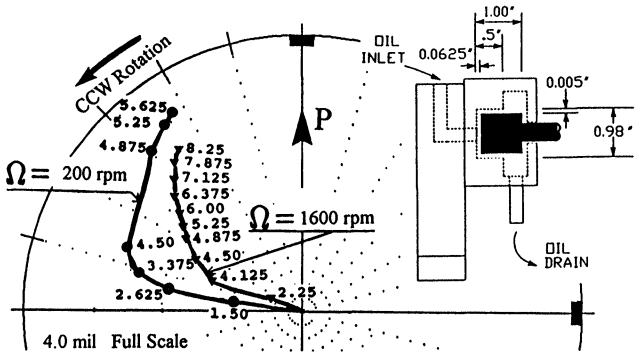

FIGURE 28 Journal centerline response to a sequence of constant vertical forces P (numbers in pounds) for two values of rotative speeds. The sketch presents the axially fed oil bearing used in this test.

IDENTIFICATION OF MULTIMODE PARAMETERS OF ROTORS USING SYNCHRONOUS PERTURBATION TECHNIQUE

Practical application of nonsynchronous perturbation in rotating machines may encounter difficulties due to limited access to the rotor for instrumentation (input force actuators and response measuring transducers).

The *synchronous* perturbation technique is simpler, although providing useful, but limited information. This technique uses shaft rotation as sweep frequency, and controlled unbalance weights as input perturbation forces. In the easiest application, the controlled unbalances may be introduced into balancing planes of the machine.

In the nonsynchronous perturbation methodology, discussed in the previous sections, the rotating force can be applied in either forward or backward directions. The controlled unbalance can rotate only in the forward direction, since it is attached to the rotor. This means that the synchronous perturbation will not provide enough data for the entire system modal parameter identification. It may bring, however, some useful information about the machine dynamics, especially when the data are taken in a time–trend sequence and, consequently, are reduced into the dynamic stiffness formats. This information may provide evidences of machine deterioration, such as wear, rotor joint looseness, rotor-to-stator rubbing, shaft cracking, and so on.

In order to eliminate the effects of other synchronous forces that possibly exist in the system, each synchronous

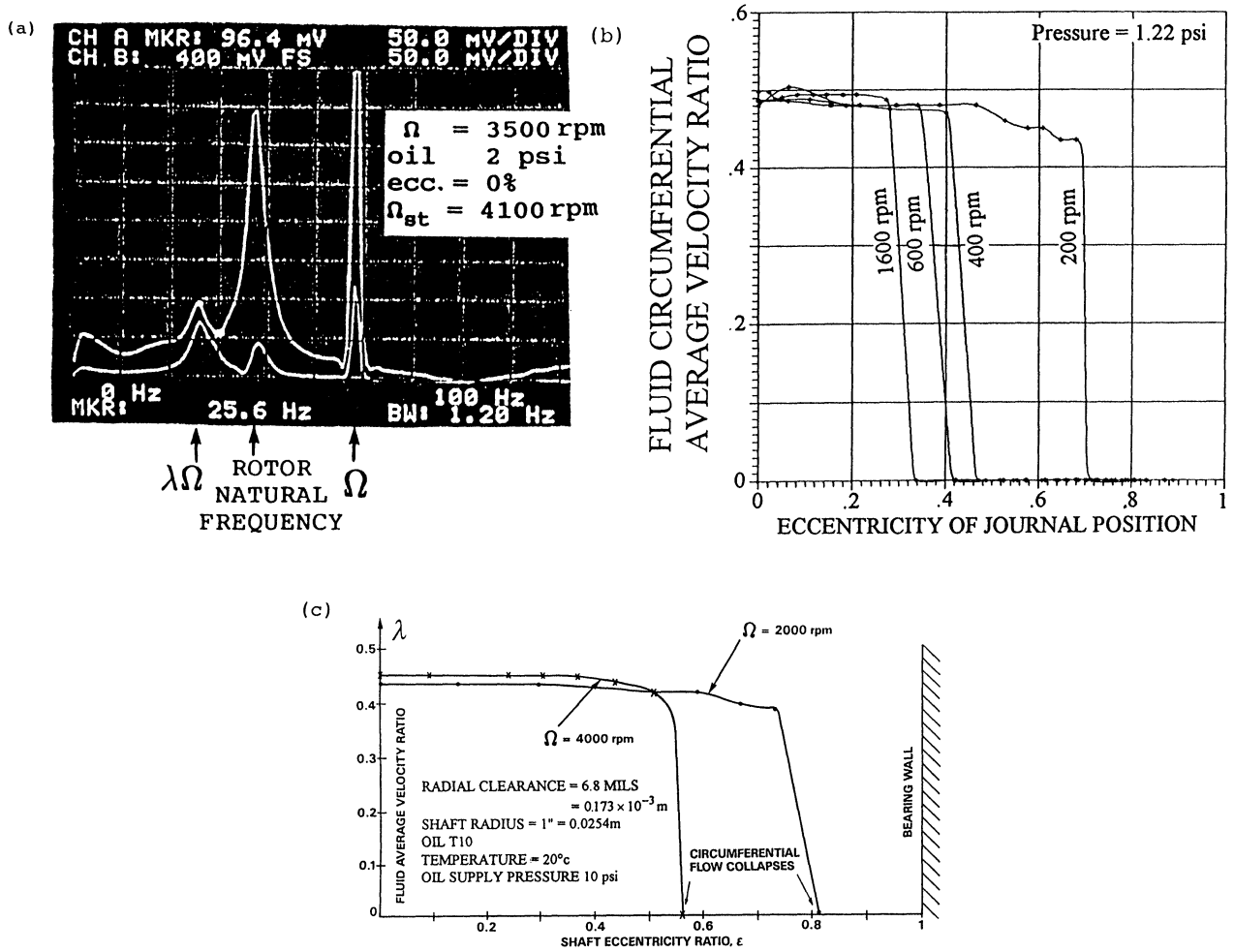

FIGURE 29 Impulse testing of rotors in fluid-lubricated bearings. (a) Example of rotor vertical and horizontal responses, a picture from the spectrum analyzer screen; synchronous vibrations (1×), whirl and "whip" natural frequencies present in the spectrum (Grant *et al.* [1992]); (b) Fluid circumferential average velocity ratio (λ) versus eccentricity ratio identified by impulse testing for the bearing illustrated in Fig. 28.; and (c)for the externally pressurized bearing (Muszynska [1988a]).

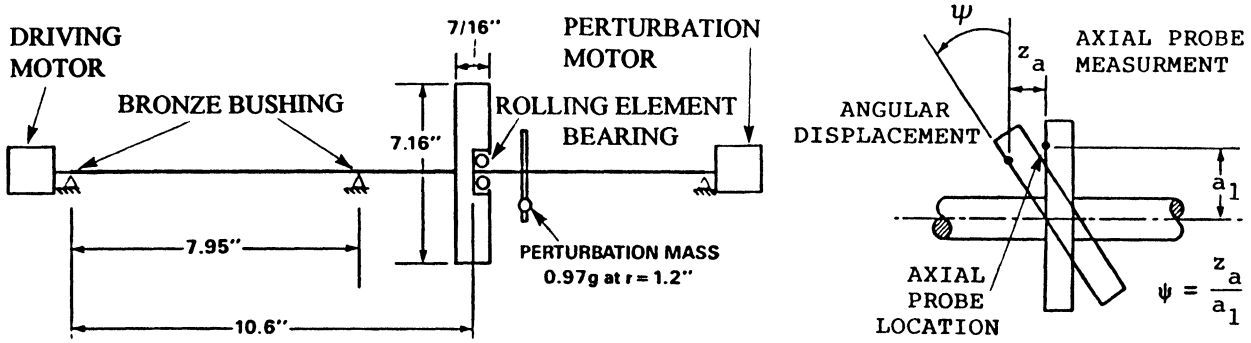

FIGURE 30 Gyroscopic rotor perturbation test rig and disk angular/axial displacement relation (Bently *et al.* [1986b]).

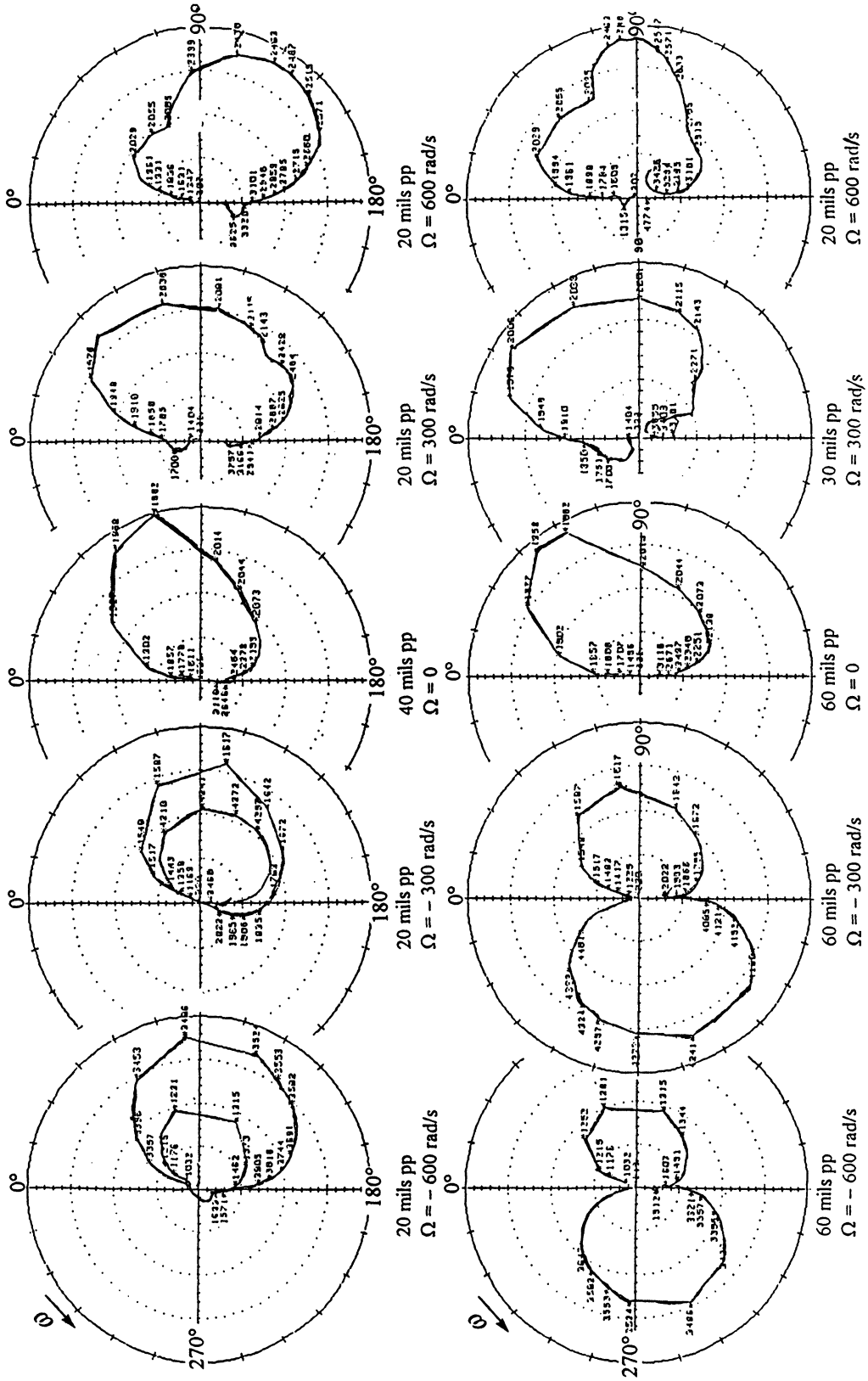

FIGURE 31 Polar plots of the rotor vertical (a) and axial (b) responses filtered to perturbation frequency for several values of the rotor rotative speeds (negative values of Ω indicate backward perturbation). Note different scales of the plots.

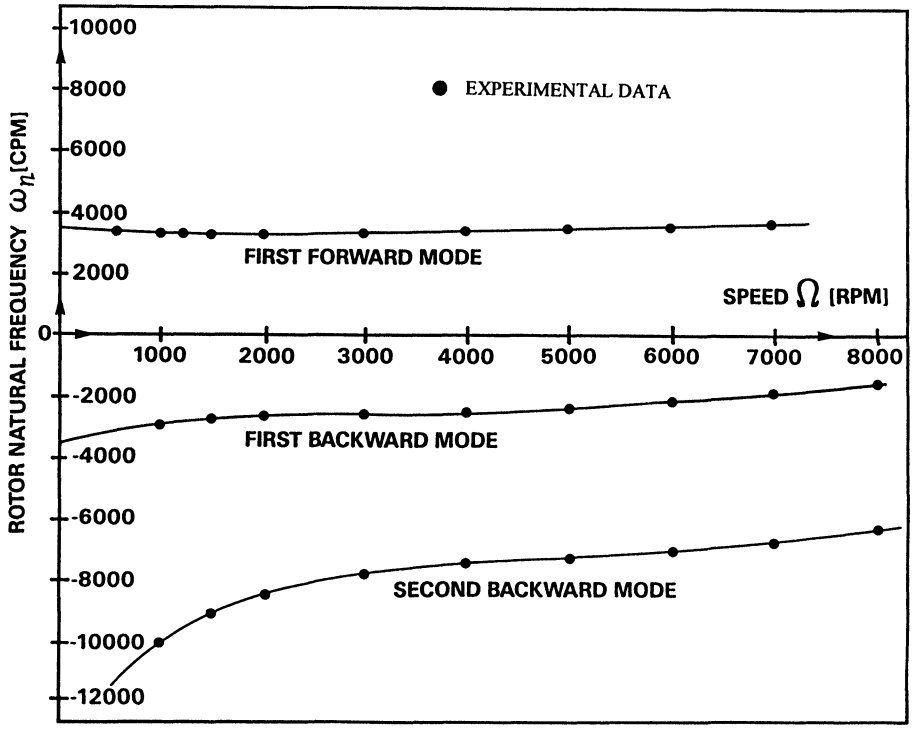

FIGURE 32 Gyroscopic rotor natural frequencies versus rotative speed obtained by nonsynchronous perturbation testing. The second forward mode occurs in the higher range of frequencies (Bently *et al.* [1986b]).

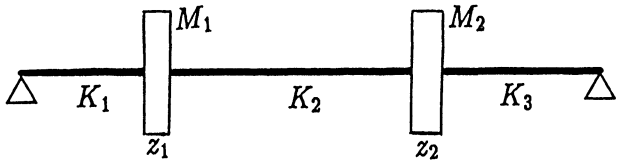

FIGURE 33 Two-mode rotor model.

perturbation test is performed twice. In the first start-up test the perturbation controlled weight is introduced to the balancing plane at certain angle δ. In the second run, the same controlled weight is moved into $\delta + 180°$ angular location at the same radius. The $1\times$ responses from these two runs are then vectorially subtracted, through the entire rotative frequency range. This eliminates the possible unknown $1\times$ components. The resulting differential data are then used for the system identification. An example of the synchronous perturbation application for two-mode rotor identification is outlined later in this section (Muszynska [1986, 1989b]).

Two-mode and, generally, coupled multimode approach, offer several advantages in comparison with the classical identification of separate mode parameters. The multimode identification provides parameters which more closely represent the structure parameters, and thus describe the system more adequately. The identification allows locating of the physical position of specific parameters most responsible for given modes. This, for instance, makes system modifications more efficient, especially when nonlinear modifications are considered. An example of formal transformation of modal variables to multi-mode modal coordinates is given at the end of this section.

The two-lateral-mode model of an isotropic rotor, the subject of synchronous perturbation, is as follows (Fig. 33):

$$\begin{bmatrix} M_1 & 0 \\ 0 & M_2 \end{bmatrix}\begin{bmatrix} \ddot{z}_1 \\ \ddot{z}_2 \end{bmatrix} + \begin{bmatrix} D_{11} & -D_{12} \\ -D_{21} & D_{22} \end{bmatrix}\begin{bmatrix} \dot{z}_1 \\ \dot{z}_2 \end{bmatrix} + \begin{bmatrix} K_1 + K_2 & -K_2 \\ -K_2 & K_2 + K_3 \end{bmatrix}\begin{bmatrix} z_1 \\ z_2 \end{bmatrix} = [F] \quad (19)$$

where $M_\nu, D_{\nu\ell}, K_\nu, \nu, \ell = 1, 2$ are rotor multimode modal masses, damping coefficients, and stiffnesses, respectively. Note that they represent partial modal parameters of the two-mode rotor. $[F]$ is the controlled synchronous perturbation force matrix. The perturbation force is applied at the first disk location in the first experiment, and at the second disk location in the second experiment (the forces and responses in the identification equations

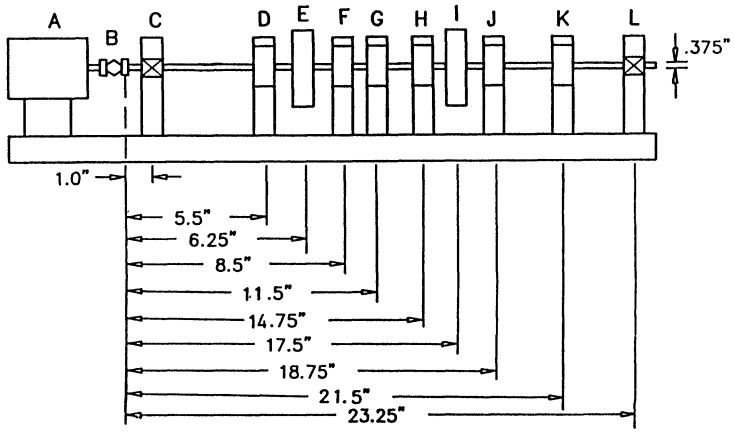

FIGURE 34 Rotor rig used for synchronous perturbation testing (Muszynska *et al.* [1989b]). *A*—electric motor, *B*—flexible coupling, *C*, *L*—inboard and outboard bronze bearing, *D*., J—inboard and outboard *XY* displacement probe mounts, *E*. *I*—inboard and outboard disks, *F*, *G*, *H*, *K*—additional displacement probes.

are actually net differential data, thus the number of necessary rotor runs is four). The matrix of the input forces resulting from two experiments is, therefore,

$$[F] = 2\begin{bmatrix} m_1 r_1 \Omega^2 e^{j(\Omega t+\delta_1)} & 0 \\ 0 & m_2 r_2 \Omega^2 e^{j(\Omega t+\delta_2)} \end{bmatrix} \quad (20)$$

where $m_\nu, r_\nu, \delta_\nu, \nu = 1, 2$ are unbalance weight mass, radius, and angular orientation, respectively, and the multiplier "2" results from the differential procedure of vectorial subtraction described above. The matrix of the system $1\times$ net responses to controlled unbalance weights for two experiments is

$$[\bar{A}] = \begin{bmatrix} A_{11}e^{j\alpha_{11}} & A_{12}e^{j\alpha_{12}} \\ A_{21}e^{j\alpha_{21}} & A_{22}e^{j\alpha_{22}} \end{bmatrix} \quad (21)$$

where $A_{\nu\ell}, \alpha_{\nu\ell}, \nu, \ell = 1, 2$ are $1\times$ amplitudes and phases, respectively, where ν represents a number of the disk where transducers are located, ℓ a number of experiment.

Following Eqs. (1) to (7), the dynamic stiffness matrix of the system (19) is calculated as

$$\begin{bmatrix} K_1+K_2+jD_{11}\Omega-M_1\Omega^2 & -K_2-jD_{12}\Omega \\ -K_2-jD_{21}\Omega & K_2+K_3+jD_{22}\Omega-M\Omega^2 \end{bmatrix}$$

$$= 2\Omega^2\begin{bmatrix} m_1 r_1 e^{j\delta_1} & 0 \\ 0 & m_2 r_2 e^{j\delta_2} \end{bmatrix}[\bar{A}]^{-1} \quad (22)$$

A flexible isotropic shaft carrying two disks, and supported in relatively rigid isotropic bearings (Fig. 34) was run with low acceleration up to 6,000 rpm. The controlled unbalance of $mr = 0.5\times 30.5$ gram $\times$ mm was installed at the inboard disk for the first run, and at the outboard disk for the second run. The rotor was equipped with one Keyphasor® probe and twelve *XY* proximity, shaft displacement observing probes at six axial locations of the shaft. The data for modal parameter identification was taken from two vertical probes only. The horizontal probes (*X*) served for checking the lateral isotropy of the rotor. The data acquisition and processing system consisted of a vector tracking filter, and the specially designed computer software. An oscilloscope and a spectrum analyzer, for additional reference checking, completed the instrumentation.

The measurements were taken at the inboard and outboard vertical locations "*D*" and "*J*" (Fig. 34). The net data resulted from vectorial subtraction of 180° and 0° controlled unbalance $1\times$ responses taken at start-up runs are illustrated in Figure 35 in the polar plot format. Figure 36 presents the direct dynamic stiffness components.

The identified values of the rotor two-mode modal parameters are as follows: $K_1 = 18900$ N/m, $K_2 = 63700$ N/m, $K_3 = 22600$ N/m, $M_1 = 0.73$ kg, $M_2 = 0.79$ kg. The estimated modal functions, basing on forced responses, are $\phi_I = 0.99$ and $\phi_{II} = -0.94$. The reduction to two modal coordinates gives two uncoupled mode modal parameters: For the first mode $M_I = M_1 + \phi_I^2 M_2 = 1.5$ kg, $K_1 = K_1 + K_2 - 2K_2\phi_I + (K_2 + K_3)\phi_1^2 = 41000$ N/m. These results coincide with the one-mode identification performed on the same rotor (Muszynska *et al.* [1989b]). For the second mode $M_{II} = M_1 + \phi_{II}^2 M_2 = 1.43$ kg, $K_{II} = K_1 + K_2 - 2K_2\phi_{II} + (K_2 + K_3)\phi_{II}^2 = 279000$ N/m.

Due to virtually low system damping, the quadrature dynamic stiffness components did not provide enough resolution to identify the damping matrix components. The modal damping coefficients D_I, D_{II} were identified from the polar plots (Fig. 35), using the half-power bandwidth

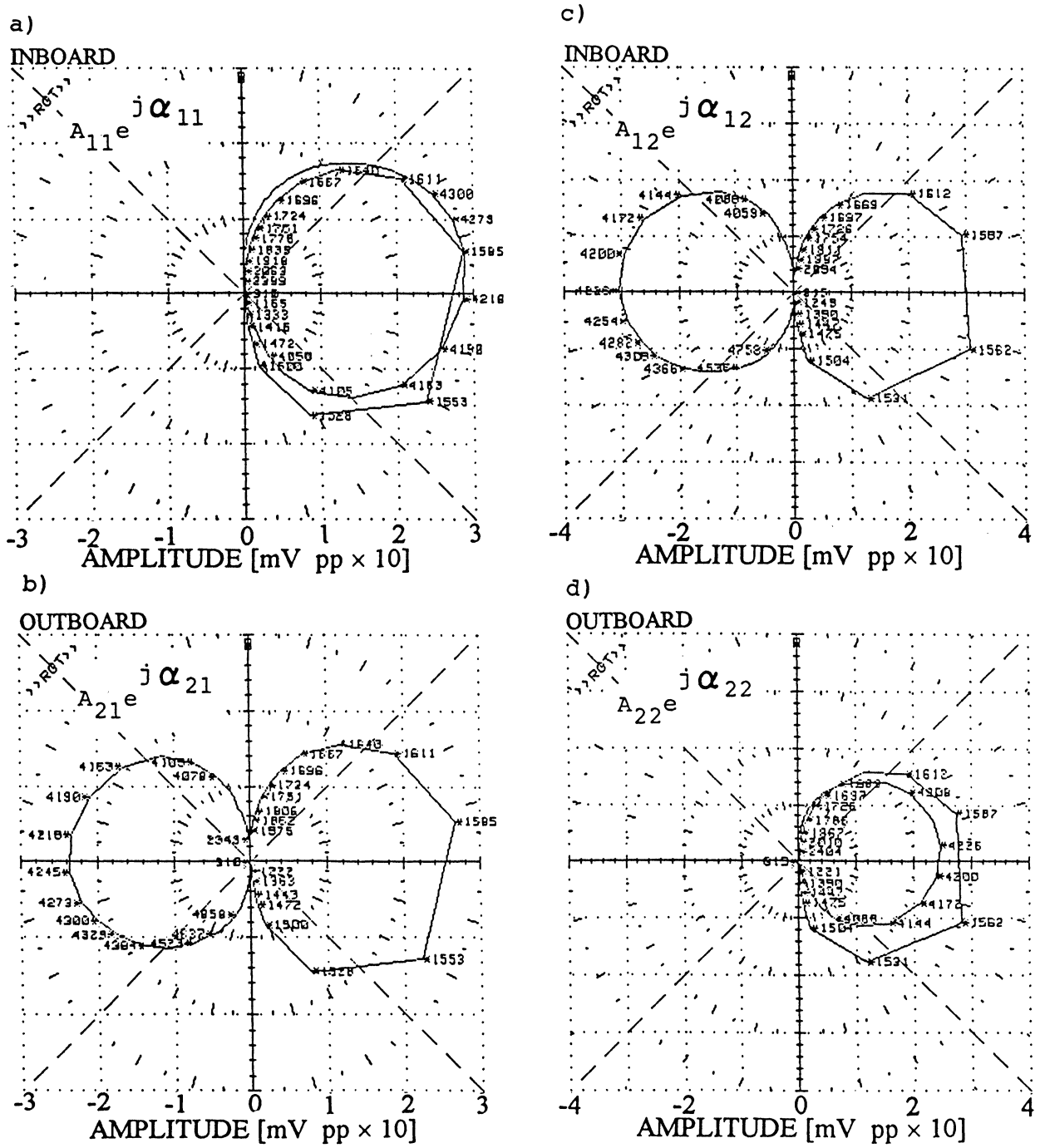

FIGURE 35 Matrix of polar plots of the rotor net synchronous response to controlled unbalance. (a), (b) unbalance at inboard disk, measurements by inboard and outboard probes, respectively, (c), (d) unbalance at outbord disk, measurements by inboard and outboard probes, respectively. Net data compensated by differential subtraction (Muszynska *et al.* [1989b]). The modal damping ratios evaluated by the half-power bandwidth method are $\zeta_I = 0.030 (D_I = 14.9$ kg/s), $\zeta_{II} = 0.032 (D_{II} = 40.4$ kg/s).

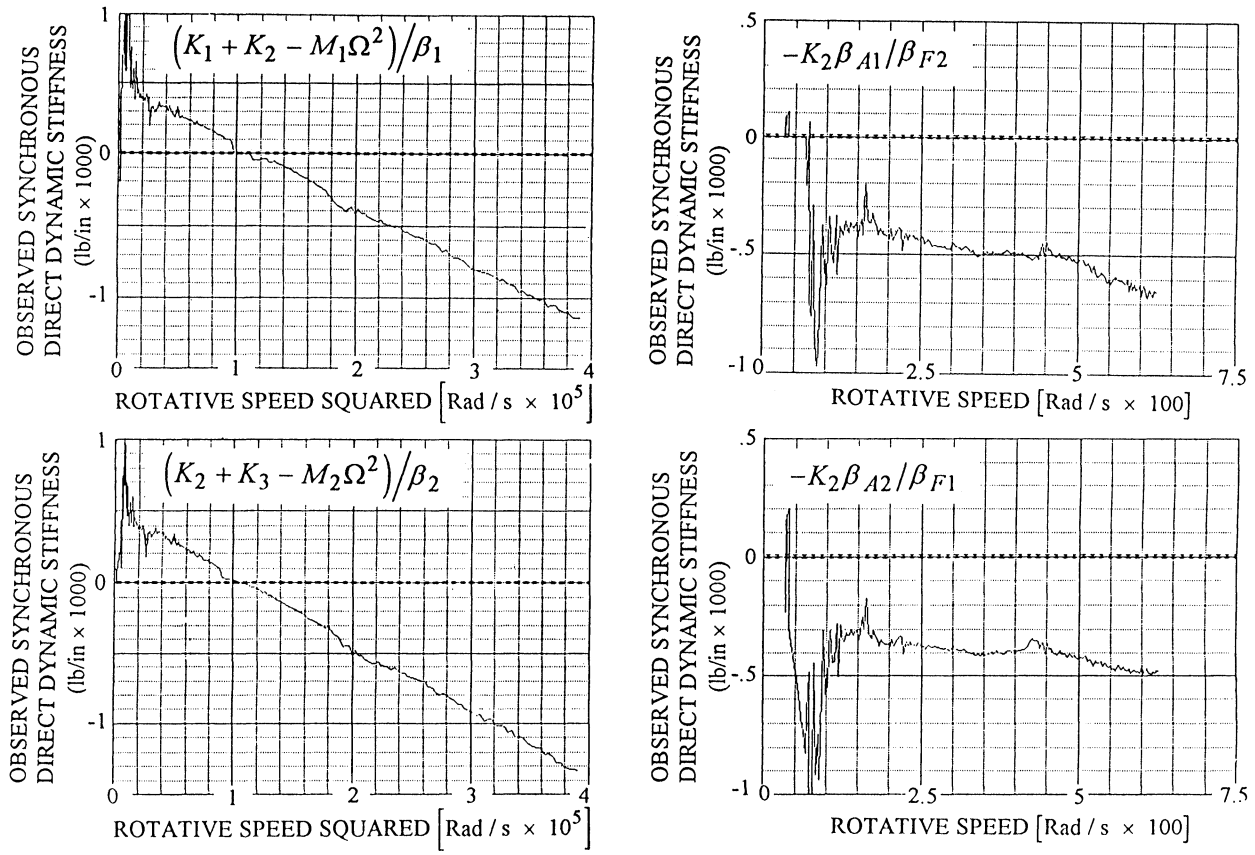

FIGURE 36 Direct dynamic stiffness components: two-mode identification of rotor parameters β's are modal correction factors (Muszynska *et al.* [1989b]).

method. The coefficients $D_{v\ell}$ of the initial damping matrix D were then calculated basing on the modal function matrix ϕ:

$$D = (\phi^T)^{-1} D_m \phi^{-1}, \qquad \phi = \begin{bmatrix} 1 & 1 \\ \phi_I & \phi_{II} \end{bmatrix}, \tag{23}$$

$$D_m = \begin{bmatrix} D_I & 0 \\ 0 & D_{II} \end{bmatrix}$$

where D_m is the diagonal modal damping matrix with elements identified using the half-power bandwidth method.

The additional proximity transducers observing the rotor served for evaluation of the modal correction factors, β. Since the two-mass rotor model (Fig. 33) is a rough approximation of the rotor behavior, and since the perturbation unbalance weights, and measuring transducers practically cannot be installed at antinodal locations, the collected data carry an error. The additional data taken from other transducers allowed for correcting this error by introducing the modal correction factors β into the final identification algorithms (Muszynska *et al.* [1989b]).

In many practical cases the limited access for installing instrumentation on a rotating machine prevents one from identifying the exact modal parameters. Very often, however, there is no need for accurate values of these parameters. Their approximate values obtained from regularly collected synchronous data (without modal correction factors β, and possible nonlinearity, and/or lateral anisotropy taken into account) represent valuable information on the machine dynamics. These values acquired in a time–trend format during the machine operation, and showing successive changes in particular dynamic stiffness components, will help in diagnosing the machine state, and in identifying the malfunction area. In addition to Bode and polar plot formats for filtered 1× vibration data reduction, the *observed dynamic stiffness* formats, which use the same raw data, provide invaluable information.

Synchronous perturbation testing is practically always done on any rotating machinery during balancing routines. The valuable dynamic stiffness data are, however, seldom appreciated, sorted out, and stored. The procedure, called here "synchronous perturbation technique," is performed during routine calibration weight balancing.

The $1\times$ response vectors during any transient start-up or shutdown should be stored, and then processed into the dynamic stiffness format versus Ω, from which the observed dynamic stiffness components, mass, stiffness, and damping, can be evaluated. If balancing is performed only at one speed, the observed dynamic stiffness will provide discrete values only.

This section will be completed with a discussion on the development of the multi-mode modal models (Muszynska, [1994]) The most often used models of mechanical structures are based on finite element grids. In rotor modeling the transfer matrix method is also used. One of the final results of these models is a set of the system natural frequencies ω_ν, $\nu = 1, \ldots, 2n$ and a set of corresponding modal functions.

The uncoupled modal variables, associated with the natural frequencies, have very little immediate correlation to the physical and geometric parameters of the system. The idea of multi-mode modeling originated from the usefulness of better correspondence of modal masses and stiffnesses to the physical system masses (such as massive disks on a rotor) and stiffnesses (such as provided by relatively slim shafts). The multi-mode model is built from the modal model. An example of its formal derivation for the case of rotor/bearing system is presented below.

The modal model obtained, for instance, from the finite element method, and possibly reduced to n modes, is as follows:

$$[M_m][\ddot{x}] + [K_m][x] = 0$$

or

$$[\ddot{x}] + \text{diag}(\omega_1^2, \ldots, \omega_n^2)[x] = 0 \qquad (24)$$

where $[x]$ is an $(n \times 1)$ rotor lateral displacement vector and $[M_m]$, $[K_m]$ are modal mass and stiffness diagonal matrices. Assume that the new multi-mode modal model of the rotor consists of n masses and $n+1$ stiffnesses connecting the masses in a chain manner. An example of such model is illustrated in Figure 33. A linear transformation $x = \psi y$ is applied to Eq. (24), with the condition that the transformed mass matrix remains diagonal, and the stiffness matrix is symmetric tridiagonal. The first condition imposes the orthogonality of the $(n \times n)$ matrix $\psi \equiv [\psi_{\mu\ell}]$:

$$\sum_{\ell=1}^{n} \psi_{\ell\mu}\psi_{\ell\nu} = \delta_{\mu\nu}, \qquad \mu, \nu = 1, \ldots, n \qquad (25)$$

where $\delta_{\mu\nu}$ is the Kronecker's delta. The condition (25) results in $n(n+1)/2$ equations for n^2 unknown elements of the matrix ψ. The transformed Eq. (24) will have the following form:

$$[\ddot{y}] + \{\psi^T \text{ diag } (\omega_1^2, \ldots, \omega_n^2)\psi\}[y] = 0 \qquad (26)$$

It is required that the matrix in parentheses { } of Eq. (26) have symmetric tridiagonal form. This condition provides additional $(n^2 - 3n + 2)/2$ equations:

$$\sum_{\ell=1}^{n} \omega_\ell^2 \psi_{\ell\mu}\psi_{\ell\nu} = 0 \qquad \text{for} \quad |\mu - \nu| > 1$$

The total number of obtained equations is $n^2 - n + 1$, thus $n-1$ of the unknown elements $\psi_{\mu\ell}$ remain arbitrary. An additional condition, which assures that the off-diagonal elements of the matrix {.} in Eq. (26) are negative, should be used:

$$\sum_{\ell=1}^{n} \omega_\ell^2 \psi_{\ell\mu}\psi_{\ell\mu+1} < 0 \qquad \text{for} \quad \mu = 1, \ldots, n-1$$

Some complementary conditions regarding the choice of matrix ψ should come from the comparison of modal deflection lines of the original model and the transformed model (26). Here there is a place for an application of optimization techniques.

PERTURBATION TESTING REVEALS LATERAL-TORSIONAL MODE CROSS COUPLING IN ROTORS

The nonsynchronous sweep frequency lateral perturbation technique has been used to investigate the lateral-torsional cross coupling due to shaft anisotropy (Bently *et al.* [1991]). The rotor of the experimental rig was driven by a synchronous electric motor, connected through a laterally flexible, torsionally rigid coupling. In order to simulate anisotropy of the shaft, a part of the shaft at mid-span was machined to produce two flats. The shaft carried two disks, with 36 gear teeth on each of them. The optical pickups observed the disk gear tooth passing frequencies. The data were then processed through a torsional signal conditioner to obtain the dynamic twist (torsional vibrations) of the shaft between two disks. The shaft lateral vibrations were observed by two sets of two proximity probes in XY configuration. The nonsynchronous perturbation unbalanced disk driven by a separate motor was attached through a rolling element bearing at the shaft mid-span.

The lateral response of the shaft to the nonsynchronous perturbation, presented in a form of the spectrum cascade plot (Fig. 37), exhibited significant amounts of the

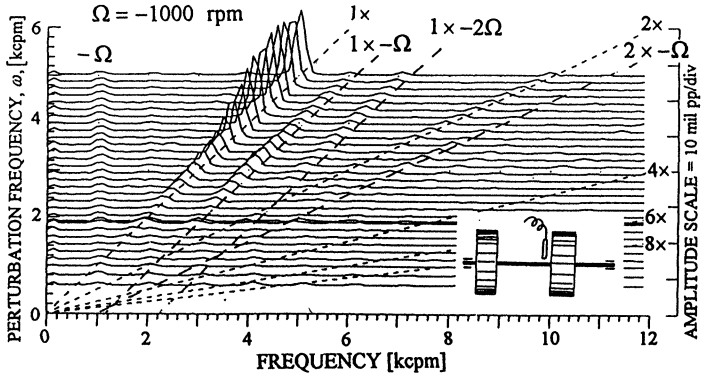

FIGURE 37 Spectrum cascade of the rotor vertical response to lateral backward rotating force nonsynchronous perturbation (Bently *et al.* [1991]; Muszynska *et al.* [1992]).

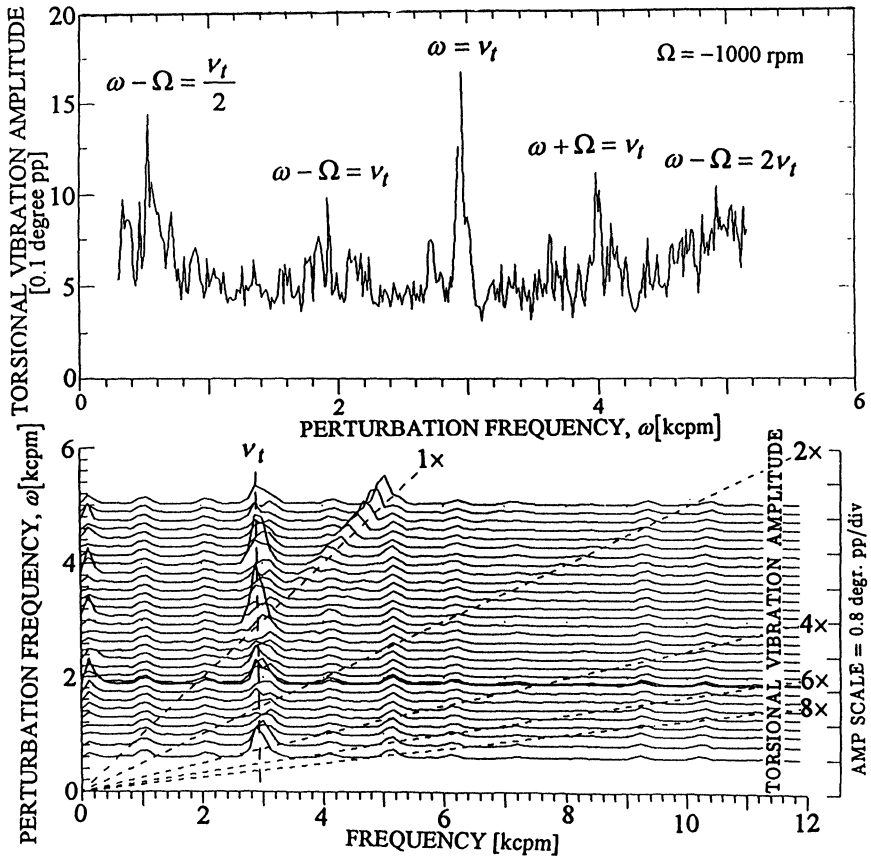

FIGURE 38 Overall amplitude versus perturbation frequency and spectrum cascade of the anisotropic rotor torsional response to lateral backward nonsynchronous perturbation (Bently *et al.* [1991]; Muszynska *et al.* [1992]). ν_t = torsional natural frequency.

frequency difference components: $\omega - \Omega$, $\omega - 2\Omega$, and $2\omega - \Omega$ (Bently *et al.* [1991]; Muszynska *et al.* [1992]). The existence of these components is due to the shaft anisotropy, and can be used for its identification. The rotor torsional responses are presented in the form of overall vibration amplitude versus perturbation frequency (Fig. 38). They exhibited high amplitudes at the excitation frequency equal to the first torsional natural frequency ν_t. The lateral/torsional coupling is related to the rotor residual unbalance. The other peaks of the torsional vibrations occur when the linear combinations of frequencies ω and Ω are equal to the torsional natural frequency ν_t and the half of

it ($\nu_t/2$). These effects are due to the asymmetry of the shaft plus radial sideload, and could also be further used for identification of the shaft anisotropy, such as could be generated by a propagating transversal crack on the shaft.

FINAL REMARKS

The sweep frequency nonsynchronous circular input force perturbation testing of rotors proved to be very powerful and efficient, producing a number of results which had not been known. The most important among them are: 1) solid/fluid interaction modes of rotors rotating in fluid environment; 2) identification of the more adequate model of fluid dynamic forces in lightly loaded bearings and in seals; and 3) multimode parameter identification of rotor/bearing/seal systems.

The nonsynchronous perturbation testing should soon be used in the routing testing of rotating machines, at first, at least, on the prototype stage. The results could provide invaluable information on fluid interaction effects on the rotor, in order to assess the stability margins from fluid whirl, whip, rotating stall, surge, and evaluate other properties of rotating machinery. Less demanding synchronous perturbation testing (known as "unbalance testing"), which is now widely performed on machines, should be accompanied by appropriate data acquisition in order to extract information on "observed dynamic stiffness." This invaluable information will greatly assist in furthering machine malfunction diagnostics by using vibration monitoring.

Nomenclature

A, α	response amplitude and phase, respectively
d	bearing diameter
D	fluid radial damping at zero eccentricity
D_s	rotor modal damping
DDS, QDS	direct and quadrature dynamic stiffness, respectively
F	force amplitude; also: fluid force
$j = \sqrt{-1}$	
H	transfer function
K, K_1, K_2, K_3	rotor modal stiffnesses
K_0	fluid radial stiffness at zero eccentricity
ℓ	bearing length
m, r, δ	unbalance mass, radius, and angular orientation, respectively
M	rotor modal mass
M_f	fluid inertia effect
p	pressure
P, γ	amplitude and angular orientation of the constant radial force used in steady-state load tests
t	time
T	temperature
x, y	rotor displacements in horizontal and vertical directions, respectively
$z = x + jy$	rotor lateral displacement in stationary coordinates
z_r	rotor lateral displacement in rotating coordinates

Greek letters

β, σ	modal correction factors
ε	eccentricity ratio
ζ	damping ratio
η	fluid dynamic viscosity
κ	complex dynamic stiffness
λ	fluid circumferential average velocity ratio
ν	natural frequency (torsional mode)
ϕ	modal function
ψ	transformation matrix; also: angular displacement coordinate
ω	perturbation frequency
Ω	rotative speed
Ω_{ST}	instability onset

Subscripts

b	bearing
d	disk
m	modal
n	number of measurement planes and number of experiments
p	measurement axial location, $p = 1, \ldots, n$; also: "perturbation"
q	displacement in "x" direction ($q = 1$) or "y" direction ($q = 2$)
r	perturbation force axial location $r = 1, \ldots, n$; also: "radial"
s	perturbation forward ($s = 1$) or backward ($s = 2$); also: "shaft"; also: "steady state"
t	tangential; also: "torsional"
μ, ν, ℓ, n	integers

References

Adams, M. L., Yang, T., and Pace, S. E., 1988, May. A Seal Test Facility for the Measurement of Isotropic and Anisotropic Linear Rotordynamic Characteristics, *Rotordynamic Instability Problems in High-Performance Turbomachinery,* The Fifth Texas A&M University Workshop, NASA CP3026, College Station, TX.

Adkins, D. R., and Brennen, C. E., 1986. Origins of Hydrodynamic Forces on Centrifugal Pump Impellers, *Rotordynamic Instability Problems in High-Performance Turbomachinery,* The Fourth Texas A&M University Workshop, NASA CP2443, College Station, TX.

Andrews, R. P., 1985. Rotor-Bearing Dynamic Analysis by Structural Decoupling, *Proceedings of the 3rd International Modal Analysis Conference,* Orlando, FL.

Bently, D. E., and Bosmans, R. F., 1979. Oil Whirl Resonance, *Fundamentals of the Design of Fluid Film Bearings,* Published by ASME.

Bently, D. E., and Muszynska, A., 1982a. Stability Evaluation of Rotor/Bearing System of Perturbation Tests, *Rotor Dynamic Instability Problems in High Performance Turbomachinery.* The Second Workshop at Texas A&M University, NASA CP2250, College Station, TX.

Bently, D. E., and Muszynska, A., 1982b. Oil Whirl Identification by Perturbation Test, *Advances in Computer–Aided Bearing Design.* 82-72978, ASME/ASLE Lubrication Conference, Washington, D.C.

Bently, D. E., and Muszynska, A., 1983. Perturbation Tests of Bearing/Seal of Evaluation of Dynamic Coefficients, *Symposium on Rotor*

Dynamical Instability, Summer Annual Conference of the ASME Applied Mechanics Division, AMD—Vol. **55,** Houston, TX.

Bently, D. E., and Muszynska, A., 1984. The Dynamic Stiffness Characteristics of High Eccentricity Ratio Bearings and Seals by Perturbation Testing, *Rotordynamic Instability Problems in High Performance Turbomachinery,* The Third Workshop at Texas A&M University, NASA CP2338, College Station, TX.

Bently, D. E., and Muszynska, A., 1985a. Identification of Bearing and Seal Dynamic Stiffness Parameters by Steady-State Load and Squeeze Film Tests, *Proeeding of BRDRC Symposium on Instability in Rotating Machinery,* NASA CP2409, Carson City, NV.

Bently, D. E., and Muszynska, A., 1985b. Measurement of Rotor System Dynamic Stiffness by Perturbation Testing, *Proceedings of BRDRC Symposium on Instability in Rotating Machinery,* NASA CP2409, Carson City, NV.

Bently, D. E., and Muszynska, A., 1985c. Perturbation Study of Rotor/Bearing System: Identification of the Oil Whirl and Oil Whip Resonances, *Proceedings of the Tenth Biennial ASME Design Engineering Division Conference on Mechanical Vibration and Noise,* 85-DET-142, Cincinnati, OH.

Bently, D. E., and Muszynska, A, 1986a. Modal Testing and Parameter Identification of Rotating Shaft/fluid Lubricated Bearing System, *Proceedings of the 4th International Modal Analysis Conference,* Los Angeles, CA.

Bently, D. E., Muszynska, A., and Olas, A., 1986b. Identification of the Modal Parameters by Perturbation Testing of a Rotor with Strong Gyroscopic Effect, *Proceedings of International Conference on Rotordynamics,* Tokyo, Japan.

Bently, D. E., Muszynska, A., and Franklin, W. D., 1988. Rotor Active 'Anti-Swirl' Control, Transactions of the ASME, *Journal of Vibration, Acoustics, Stress and Reliability in Design,* Vol. **110,** No. 2.

Bently, D. E., Muszynska, A., and Goldman, P., 1991. Torsional/Lateral Vibration Cross Coupling Due to Shaft Asymmetry, *BRDRC Report No. 1.*

Bigret, R., 1984. Elements for the Modal Analysis of Symmetric and Non-Symmetric Transfer Matrix Structures, *Proceedings of the 2nd International Modal Analysis Conference,* Orlando, FL.

Black, H. F., 1969. Effects of Hydraulic Forces in Annular Pressure Seals on the Vibrations of Centrifugal Pump Rotors, *Journal of Mechanical Engineering Science,* Vol. **II,** No. 2.

Black, H. F., and Brown, R. D., 1980. Modal Dynamic Simulation of Flexible Shafts in Hydrodynamic Bearings, *Vibration in Rotating Machinery,* Proceedings of IMechE Conference, C266/80, Cambridge, UK.

Black, H. F., and Jensen, D. N., 1970. Dynamic Hybrid Bearing Characteristics of Annular Controlled Leakage Seals, *Proceedings of Institution of Mechanical Engineers,* Vol. **184.**

Bolotin, V. V., 1963. *Nonconservative Problems in the Theory of Elastic Stability,* Macmillan, New York.

Brennen, C. E., Franz, R., and Arndt, N., 1988. Effects of Cavitation on Rotordynamic Force Matrices, *Proceedings of 1988 Conference on Advanced Earth-to-Orbit Propulsion Technology,* NASA CP3012, Huntsville, AL.

Childs, D. W., 1976. A Modal Transient Simulation Model for Flexible Asymmetric Rotors, Transactions of the ASME, *Journal of Engineering of Industry,* No. 2.

Childs, D. W., 1986. Force and Moment Rotordynamic Coefficients for Pump–Impeller Shround Surfaces, *Rotordynamic Instability Problems in High Performance Turbomachinery,* The Fourth Texas A&M University Workshop, NASA CP2443, College Station, TX.

Childs, D. W., Elrod, D., and Hale, K., 1988. Annular Honeycomb Seals: Test Results for Leakage and Rotordynamic Coefficients, Comparison of Labyrinth and Smooth Configurations, *Rotordynamic Instability Problems in High Performance Turbomachinery,* The Fifth Texas A&M University Workshop, NASA CP3026, College Station, TX.

Ewins, D. J., 1984. Modal Testing: Theory and Practice, Research Studies Press Ltd., John Wiley & Sons, New York.

Fillod, R., Piranda, J., and Bonnecase, D., 1985. Taking Nonlinearities into Account in Modal Analysis by Curve Fitting of Transfer Function, *Proceeding of the 3rd International Modal Analysis Conference, Orlando, FL.*

Glasgow, D. A., and Nelson, H. D., 1980. Analysis of Rotor/Bearing Systems Using Component Mode Synthesis, Transactions of the ASME, *Journal of Mechanical Design,* Vol. **102.**

Grant, J. W., 1991. Modelling and Stabilization of a Rotor Supported in a Fluid Bearing, M. Sci. Dissertation, University of Nevada, Reno.

Grant, J. W., and Huang, X., 1992. Perturbation Testing of a Rotor/Bearing System with Various Stability Thresholds Due to Changes in Lubricant Pressure, *BRDRC Report No. 4.*

Hull, E. H., 1955. Journal Bearing Behavior Under Periodic Loading, G. I. Research Laboratory, Rep. No. 55–RL–1354, Schenectady, NY.

Iwatsubo, T., 1980. Evaluation of Instability Forces of Labyrinth Seals in Turbines or Compressors, *Rotordynamic Instability Problems in High-Performance Turbomachinery,* The First Texas A&M University Workshop, NASA CP2133, College Station, TX.

Iwatsubo, T., Sheng, B., and Matsumoto, T., 1988. An Experimental Study on the Static and Dynamic Characteristics of Pump Annular Seals, *Rotordynamic Instability Problems in Hih-Performance Turbomachinery,* The Fifth Texas A&M University Workshop, NASA CP3026, College Station, TX.

Jery, B., Acosta, A. J., Brennen, C. E., and Caughey, T. K., 1984. Hydrodynamic Impeller Stiffness, Damping, and Inertia, *Rotordynamic Instability Problems in High-Performance Turbomachinery,* The Third Texas A&M University Workshop, NASA CP2338, College Station, TX.

Kanki, H., Fujii, H., Hizume, A., Ichimura, T., and Yamamoto, T., 1986. Solving Nonsynchronous Vibration Problems of Large Rotating Machineries by Exciting Test in Actual Operating Condition, *Proceedings of International Conference on Rotordynamics,* Tokyo, Japan.

Muszynska,A., 1986. Whirl and Whip—Rotor/Bearing Stability Problems, *Journal of Sound and Vibration,* Vol. **110,** No. 3.

Muszynska, A., 1988a. Improvements in Lightly Loaded Rotor/Bearing and Rotor/Seal Models, Transactions of the ASME, *Journal of Vibration, Acoustics, Stress, and Reliability in Design,* Vol. **110,** No. 2.

Muszynska, A., 1988b. Modal Testing of Rotor/Bearing Systems, *International Journal of Analytical and Experimental Modal Analysis,* Vol. **1,** No. 3.

Muszynska, A., 1988c. Multimode Whirl and Whip in Rotor/Bearing Systems, *Dynamics of Rotating Machinery,* Vol. **2,** Hemisphere Publishing, Proceedings of Second International Symposium on Transport Phenomena, Dynamics, and Design in Rotating Machinery, Honolulu, HI.

Muszynska, A., and Bently, D. E., 1989a. Anti–Swirl Arrangements Prevent Rotor/Seal Instability, Transactions of the ASME, *Journal of Vibration, Acoustics, Stress and Reliability in Design,* Vol. **111,** No. 2.

Muszynska, A., and Bently, D. E., 1990. Frequency Swept Rotating Input Perturbation Techniques and Identification of the Fluid Force Models in Rotor/Bearing/Seal Systems and Fluid Handling Machines, *Journal of Sound and Vibration,* Vol. **143,** No. 1.

Muszynska, A., Bently, D. E., Franklin, W. D., and Hayashida, R. D., 1989b. Identification of Modal Parameters of Rotating Systems Using Perturbation Techniques, Part 2, *Proceedings the 12th Biennial ASME Conference on Mechanical Vibration and Noise,* Montreal, Canada.

Muszynska, A., Bently, D. E., Franklin, W. D., Grant, J. W., and Goldman, P., 1993, April. Applications of Sweep Frequency Rotating Force Perturbation Methodology in Rotating Machinery for Dynamic Stiffness Identification, Transactions of the ASME, Journal of Engineering for Gas Turbines and Power, V. 115.

Muszynska, A., 1994, Application of Multi-Mode Modal Models in Rotor Dynamics, ISROMAC–5, Hawai.

Ohashi, H., 1984. Lateral Fluid Forces Acting on a Whirling Centrifugal Impeller in Vaneless and Vaned Diffuser, *Rotordynamic Instability Problems in High-Performance Turbomachinery,* The Third Texas A&M University Workshop, NASA CP2338, College Station.

Ohashi, H., Sakurai, A., and Nishihama, J., 1988. Influence of Impeller and Diffuser Geometries on the Lateral Fluid Forces of Whirling Centrifugal Impeller, *Rotordynamic Instability Problems in High–Performance Turbomachinery,* The Fifth Texas A&M University Workshop, NASA CP3026, College Station, TX.

Stone, J. M., and Underwood, F. A., 1947. Load Carrying Capacity of Journal Bearings, *SAE Quartarly Transactions,* No. 1.

Sullivan, B. J., 1985. Application of Modal Superposition in Nonlinear Rotor Dynamic Analysis, *Proceedings of the 3rd International Modal Analysis Conference,* Orlando, FL.

Zhang, Q., and Lallement, G., 1985. Experimental Determination of Eigen Solutions of Nonself-Adjoint Mechanical Structures, *Proceedings of the 3rd International Modal Analysis Conference,* Orlando, FL.